A mixture-like model for tumor-immune system interactions

Christian Tayou Fotso, Simon Girel, Fabienne Anjuère, Véronique M Braud, Florence Hubert, Thierry Goudon

Highlights

A mixture-like model for tumor-immune system interactions*

Christian Tayou Fotso, Simon Girel, Fabienne Anjuère, Véronique M. Braud, Florence Hubert, Thierry Goudon

- A new model based on mixture theory for describing the tumor growth and immune response interactions
- Reproduction of elimination/equilibrium and escape phases
- Crucial role of the access to nutrients and protumor immune effects in favoring tumor expansion

A mixture-like model for tumor-immune system interactions

Christian Tayou Fotso[a], Simon Girel[a], Fabienne Anjuère[b], Véronique M. Braud[b], Florence Hubert[c], Thierry Goudon[a,*]

[a] *Université Côte d'Azur, Inria, CNRS, LJAD, Parc Valrose, F-06108, Nice, France*
[b] *Université Côte d'Azur, CNRS, Institut de Pharmacologie Moléculaire et Cellulaire UMR 7275, 660 Route des Lucioles, F-06560, Valbonne, France*
[c] *I2M, Aix Marseille Université, CNRS, 39 rue F. Joliot-Curie, F-13453, Marseille, France*

Abstract

We introduce a mathematical model based on mixture theory intended to describe the tumor-immune system interactions within the tumor microenvironment. The equations account for the geometry of the tumor expansion, and the displacement of the immune cells, driven by diffusion and chemotactic mechanisms. They also take into account the constraints in terms of nutrient and oxygen supply. The numerical investigations analyze the impact of the different modeling assumptions and parameters. Depending on the parameters, the model can reproduce elimination, equilibrium or escape phases and it identifies a critical role of oxygen/nutrient supply in shaping the tumor growth. In addition, antitumor immune cells are key factors in controlling tumor growth, maintaining an equilibrium while protumor cells favor escape and tumor expansion.

Keywords: Cancer growth, Immune response, Mixture models
2000 MSC: 35Q92, 76T99, 76Z99, 92C50

⋆This work is supported by the "Mission pour les initiatives transverses et interdisciplinaires" of CNRS, as a laureate of the program "80Primes". This work is equally supported by the French Government (National Research Agency, ANR) through the Investments for the Future programs LABEX SIGNALIFE ANR-11-LABX-0028 and IDEX UCAJedi ANR-15-IDEX-01.

*Corresponding author
Email address: thierry.goudon@inria.fr (Thierry Goudon)

1. Introduction

The tumor microenvironment (TME) is a central dynamic and complex cellular and acellular milieu that influences tumor growth kinetics. Within the TME, it is well established that the immune system plays a central role in the maintenance of the organisms integrity by continuously eliminating newly produced transformed cells, a concept called cancer immunosurveillance composed of three phases: Elimination – tumor cells are simply destroyed by the immune response –, Equilibrium – the immune system maintains and controls the tumor in a viable state – and Escape – with the unlimited growth of the tumor –. This last phase results from a cancer immunoediting exerted by the immune system and from the establishment of immune suppression mechanisms [28, 29, 34]. Indeed, cancer cells can also turn immune responses at their own advantage, transforming immune cells to protumoral cells stimulating tumor development. The success of immunotherapies is based on the attempt to maintain or reverse this balance towards the "Equilibrium" and "Elimination" phases [10]. Unfortunately, these approaches show clinical efficacy with durable responses in only 15-20% of all cancer patients so far. Despite intense research, these treatment failures are currently poorly explained.

Technological developments at the single cell level have helped to better understand the complexity of the TME. Tumor cells lay in a microenvironment composed of immune cells, cancer-associated fibroblasts (CAF), extracellular matrix proteins that form the stroma, blood and lymphatic vessels and nerve fibers [4]. The composition and spatial organization of the TME can vary greatly between tumors and even within a given lesion. In invasive cutaneous squamous cell carcinoma (cSCC), the second deadliest skin cancer with no curative therapy available following successive relapses, a strong immune infiltrate has been detected [12, 37, 42]. To better visualize all the components of the cSCC TME, new imaging mass cytometry techniques have been developed that allowed the simultaneous detection of up to 40 markers [32]. The obtained images show tumor islets surrounded by stroma rich in ECM proteins and immune cells. Mathematical models and numerical simulations can provide relevant information, complementary to experimental and clinical observations, that can help to understand the underlying biological mechanisms within the TME.

Many mathematical models have been introduced so far with quite elaborate descriptions of the tumor-immune interactions based on systems of

ordinary differential equations, see for instance [25, 26, 30, 31, 38, 39]. However, the spatial repartition of the tumor and immune cells seems to play a crucial role [27] and cannot be easily taken into account by such ODE systems. For instance, this observation has motivated the work detailed in [1, 5, 6, 7]. Therefore, we adopt a different viewpoint and we are going to set up a continuous model based on partial differential equations, describing the tumor growth and the immune response by considering the cell densities, and unknowns that depend on both the time t and the position x. To this end, we shall describe the tumor and immune cell interactions by means of fluid mechanic principles, appealing to methods of mixture theory [49] and their application to biological flows [20, 46]. This approach, which takes inspiration from [3, 11, 13, 14, 17, 21, 22, 35, 47, 48] for applications to tumor growth, is intended to consider more precisely the tumor microenvironment geometry, and the infiltration of the tumor by the immune cells. The fluid mechanic principles will be combined with the interaction mechanisms with immune cells identified in our previous works[1] [5, 6, 7] namely:

- Recruitment and activation of immune cells, from a bath and sources of "naive" immune cells, are governed by the tumor growth;
- Chemotactic effects drive the immune cells towards the tumor microenvironment;
- Tumor cells are destroyed by antitumor immune cells (NK and CD8+ T cells);
- antitumor functions can be inhibited by protumor immune cells and shifted from antitumoral to protumoral activities;
- The tumor growth rate can be enhanced by activated protumor immune cells.

Furthermore, these mechanisms have to be coupled with the description of how the tumor grows at the expense of its environment (fluids, fibers, extracellular matrix), and the complex mechanisms relying on the activation of cancer associated fibroblasts. The model should take into account the access

[1]Even though [5, 6, 7] are concerned with completely different models, of more microscopic nature, more adapted to the earliest stages of the tumor growth. In the same vein, we also refer the reader to [1].

to nutrient and oxygen, that determines the proliferation rate, and can even lead to necrosis when it becomes insufficient. Therefore, the equations are established through the combination of mechanical and biological effects that govern the competition for space and resources between different species of cells. In particular, the coupling between the different constituents of the TME not only arises through the mass exchange dynamics, but also in the momentum balance, that involves a description of the mechanical forces on a given phase (viscosity, pressure, friction between the phases). Finally, the model is closed by an algebraic constraint, which enters into the definition of the pressure field. In order to ease the access to the equations, a schematic view of the main principles at the basis of the proposed model is offered in Figure 1 and 2, whereas Table 1 collects the definition of the unknowns.

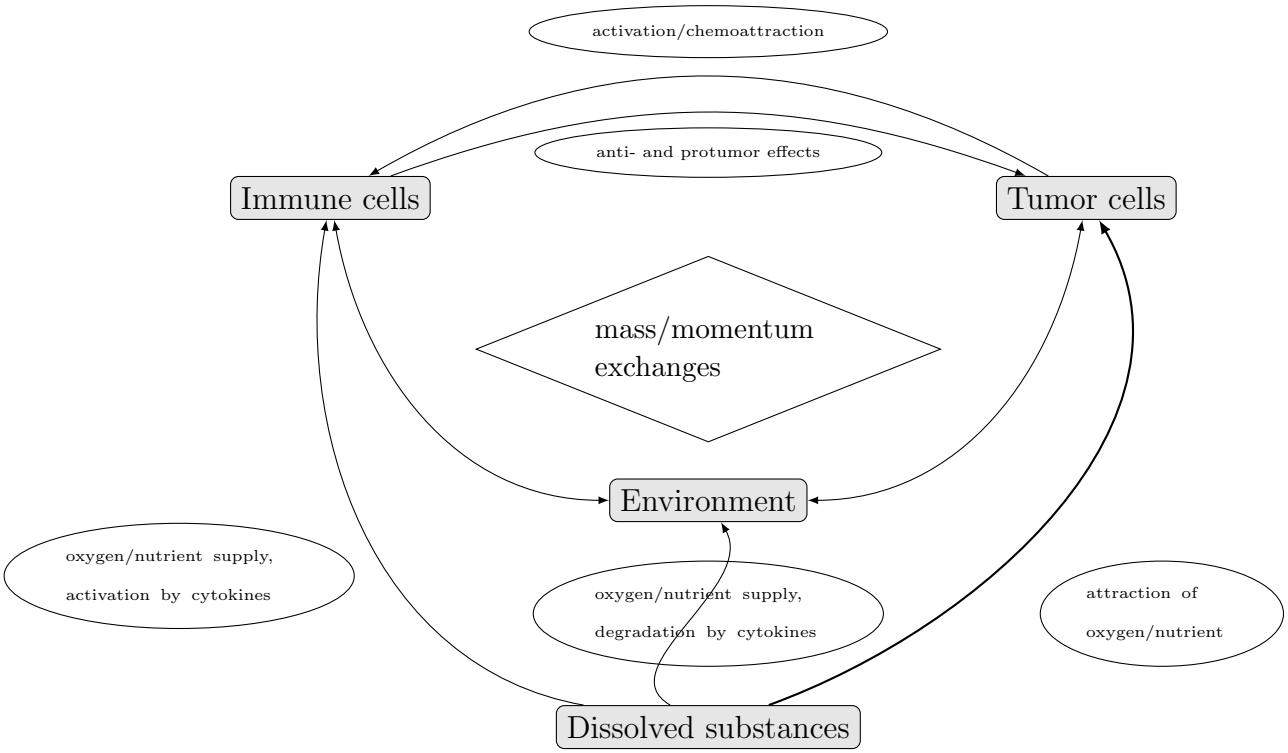

Figure 1: Competition for space and resources, a schematic view of the main mechanisms

Having set up the model, the aim of this preliminary study is to discuss the influence of the modeling assumptions and try to hierarchize through

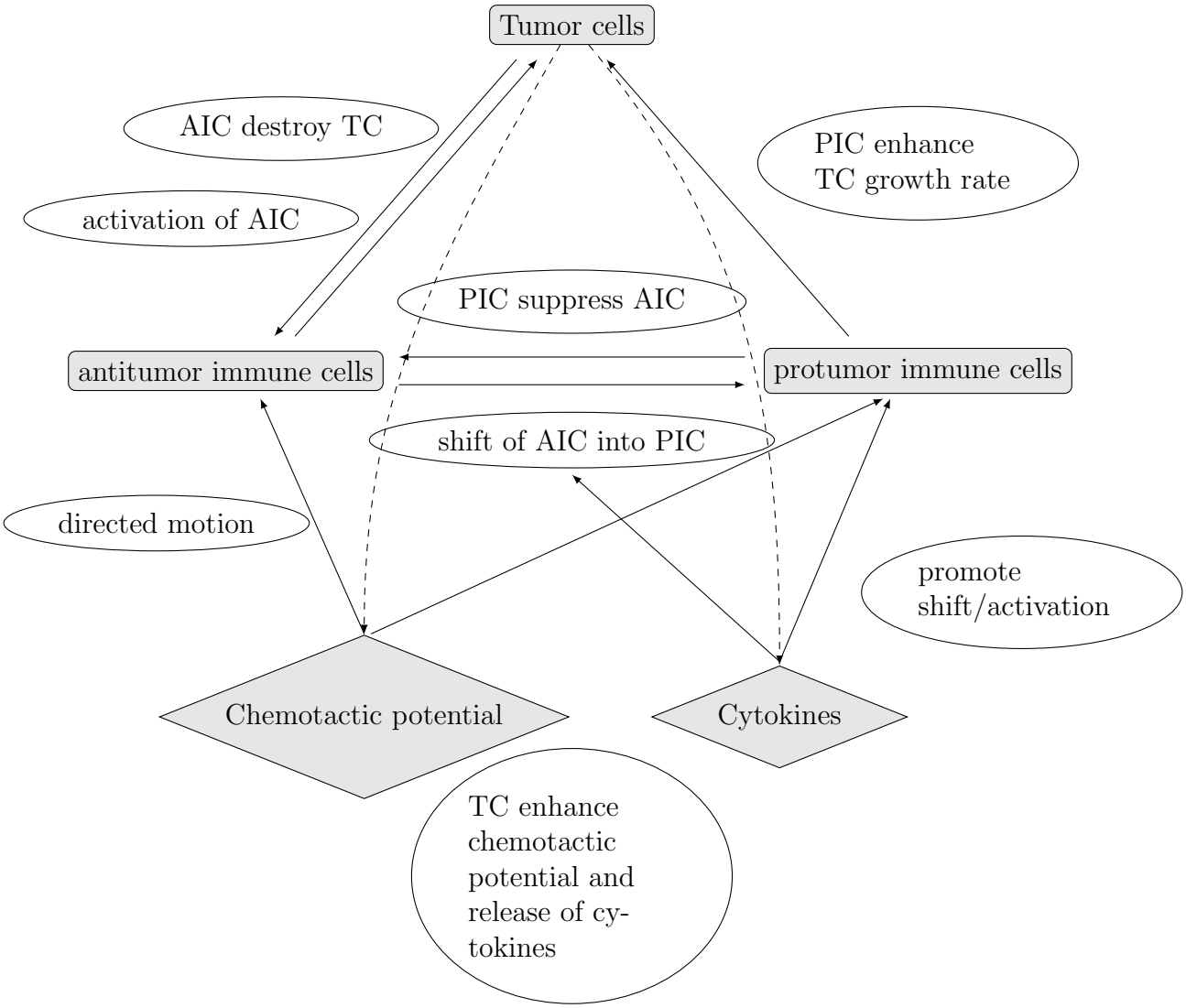

Figure 2: Tumor and immune cells interactions. AIC: antitumor cells, PIC: protumor cells, TC: tumor cells. See Table 1 for definition and notation of the associated unknowns

simulations the effects of the biological and mechanical mechanisms, to assess whether or not the model is able to reproduce equilibrium and escape phases, and to shed some light on the critical phenomena that shape the space organization of the TME. The paper is organized as follows. In Sec-

tion 2 we introduce in details the system of equations that is intended to describe the interactions between the tumor growth, the immune response, and the environment. In Section 3, we discuss several simplified versions of this complex system and, based on numerical experiments, the role of the modeling assumptions and parameters. Our main conclusions are the following. Firstly, oxygen/nutrient supply is critical for shaping the tumor development. Secondly, the various versions of the model are able to reproduce the "3E" phases; in particular equilibrium phases with a residual tumor remaining under the control of the immune system can be observed. Thirdly, taking into account protumoral effects of the immune response dramatically changes the dynamic and might lead to the unlimited tumor expansion.

2. Model description

We adopt a modeling where we distinguish two types of populations:

- the "constituents", a set which contains the tumor, the (anti- and protumor) immune cells and at least another population describing the "environment" (other cells and tissues, extracellular matrix and interstitial fluid...). These interacting phases are described by their volume fractions, hereafter denoted ϕ_j for $j \in \{1, ..., J\}$. Quoting [3], *In a continuum description, the "number of cells" of a given species is probably not a suitable candidate: it seems more appropriate to introduce the volume fraction concept, straightforwardly inherited from the theory of multicomponent continua, so that "balance equations" for the components are to be read as "mass balance equations". Such a set of equations obviously calls for velocity (or displacement) fields that are to be enforced somehow.* The concept of mixture flows precisely means that at each space point, a fraction (given by ϕ_j) of each phase can be encountered. The general form of the mass balance equations is

$$\partial_t(\rho_j \phi_j) + \nabla_x \cdot \mathscr{J}_j = \Gamma_j, \tag{1}$$

where ρ_j is the typical mass density of the phase j. It is assumed to be a positive constant (incompressibility assumption for each phase). Very likely these positive quantities have similar values, which would allow us to simplify the equations: quite often it is assumed that all ρ_j's are given by the mass density of water, see [3] for instance. The modeling issue relies in finding a relevant expression for

– the mass exchange term Γ_j, which can naturally be split into gain and loss terms

$$\Gamma_j = Q_j - \rho_j \phi_j L_j$$

where Q_j and L_j are non negative functions of the physical quantities of the model (this formulation is related to the preservation of the natural property $\phi_j \geq 0$);

– the mass fluxes $\mathscr{J}_j$ can be written as

$$\mathscr{J}_j = \rho_j \phi_j V_j \tag{2}$$

and we shall derive a relevant expression for the velocity field V_j. As we shall see below it might induce a combination of convection and diffusion effects.

- the "substances" like nutrient , oxygen, cytokines and chemokines... which are described by their concentration α_k, $k \in \{1, ..., K\}$. They are considered as components dissolved in the mixture. The concentrations obey convection-diffusion equations, with reaction terms accounting for gain and loss processes.

Such a distinction appears for instance in [3, 48, 52], or, in different contexts, in [40, 46]. Simplifying assumptions can be used to reduce the model, skipping difficulties related to determining the displacement of the cells in terms of the other unknowns and reducing the description to a mere ODE for the radius of a radially symmetric tumor [3, 41]. A crucial feature of the model is that, according to the definition of the unknowns as volume fractions, the relation

$$\sum_{j=1}^{J} \phi_j = 1 \tag{3}$$

holds. This property has two important consequences for the derivation of the equations. First of all, summing all mass balance equations (1), one is led to a constraint on the mean volume velocity

$$\nabla_x \cdot \left(\sum_{j=1}^{J} \frac{\mathscr{J}_j}{\rho_j} \right) = \nabla_x \cdot \left(\sum_{j=1}^{J} \phi_j V_j \right) = \sum_{j=1}^{J} \frac{\Gamma_j}{\rho_j}. \tag{4}$$

This constraint implicitly defines a Lagrange multiplier, which induces a pressure field Π. Second of all, this constraint has to be taken into account

for the set up of the boundary conditions, which should be consistent with (4) in the sense that

$$\int_{\partial\Omega} \sum_{j=1}^{J} \frac{\mathscr{J}_j}{\rho_j} \cdot \nu_x \, \mathrm{d}\sigma_x = \int_{\Omega} \sum_{j=1}^{J} \frac{\Gamma_j}{\rho_j} \, \mathrm{d}x, \tag{5}$$

holds, with ν_x the outward unit normal at $x \in \partial\Omega$.

2.1. Mass exchange terms and constituents' equations

2.1.1. Mass exchange for the immune cells

We denote with a subscript a, resp. p, physical quantities associated to the antitumor immune cells (like NK and CD8+ T cells, tumor-associated neutrophils TAN-N1, tumor-associated macrophages M1), resp. protumor immune cells (like Treg, MDSCs, TAN-N2 and TAM-M2); similarly we refer to the tumor and the environment with the subscripts n and m, respectively. For the mass exchange terms, the following actions are retained from [5]

- both anti and protumor cells are subjected to natural death, with rates (homogeneous to the inverse of a time) γ_a, γ_p respectively;
- antitumor cells are activated from a source S_a, at a rate that depends on the total tumor mass

$$\mu_n = \int \rho_n \phi_n \, \mathrm{d}x; \tag{6}$$

- cytokines, or more generally protumoral factors, are characterized by a concentration denoted by I; they promote the shift of antitumor cells into protumor cells in the vicinity of the tumor[2], as well as the activation of protumor cells from a source S_p;
- protumor cells annihilate antitumor cells.

Note that the sources of antitumor S_a and protumor S_p immune cells can be space dependent, and different both in amplitude and localization, describing specific sites of recruitment (like the lymph nodes for T cells, or the bone marrow for protumor cells), see [6].

[2]There are also cytokines with antitumor effects, but they are not considered as such in the model.

Hence, the mass exchanges terms for the antitumor and protumor immune cells are given by

$$\Gamma_a = \rho_a\Big(g(\mu_n)S_a - \phi_a\Big(\gamma_a + k_{Ia}I + \frac{\phi_p}{\tau_{ap}}\Big)\Big), \tag{7}$$

and

$$\Gamma_p = k_{Ip}I\rho_p S_p + \rho_a\phi_a k_{Ia}I - \gamma_p\rho_p\phi_p, \tag{8}$$

respectively. In these expressions, all coefficients $\gamma_a, \gamma_p, 1/\tau_{ap}, k_{Ia}I, k_{Ip}I$ are homogeneous to the inverse of a time. The function $g : [0,\infty) \to [0,\infty)$, which equally has the homogeneity of the inverse of a time, is the tumor mass dependent activation rate of effector cells from the bath of resting immune cells; the activation law can incorporate relevant limitation mechanisms, for instance based on Michaelis-Menten kinetics. In what follows we adopt a simple linear relation $g(\mu_n) = g_0\mu_n$, with $g_0 > 0$.

Protumoral effects involve the action of cytokines/protumoral factors; according to [5], the evolution of cytokine concentration is driven by a mere ODE

$$\frac{\mathrm{d}}{\mathrm{d}t}I = \psi - \frac{I}{\tau}, \tag{9}$$

with $\tau > 0$ a relaxation time and ψ a threshold function (for instance proportional to $(\phi_n - \phi_c)_+$ for some $\phi_c \geq 0$). Here, the concentration I can describe further protumor signals, immunosuppressive cytokines and Cancer Associated Fibroblasts (CAF). In this case, we slightly modify the modeling by assuming that ψ depends on the tumor volume fraction ϕ_n and the environment volume fraction ϕ_m, with

$$\psi(\phi_n = 0, \phi_m) = 0, \qquad \psi(\phi_n, \phi_m = 0) = 0.$$

For instance, we can set

$$\psi(\phi_n, \phi_m) = \frac{[\phi_n - \phi_{n_{I,s}}]_+[\phi_m - \phi_{m_{I,s}}]_+}{\tau}$$

with some thresholds $\phi_{n_{I,s}}, \phi_{m_{I,s}}$. It means that the production of cytokines/protumoral factors need a sufficiently large presence of both tumor cells and environmental cells to be triggered. This simple ODE is a simplified modeling that neglects convection and diffusion effects.

2.1.2. Mass exchange for the tumor

Cell proliferation is limited by the competition for space, which is described through the homeostatic pressure, [8]. This effect is taken into account through a (non negative and increasing) function $\mathscr{P}$ of the tumor volume fraction ϕ_n, and a threshold ϕ_*. A typical choice is

$$\mathscr{P} = \frac{\nu p_*}{\nu - 1}\Big(\frac{\phi_n}{\phi_*}\Big)^{\nu-1}, \qquad \nu > 1, \qquad 0 < \phi_* < 1, \qquad p_* > 0, \tag{10}$$

see [23, 45]. Here, p_* is a reference pressure, which has the homogeneity of $\big(\frac{length}{time}\big)^2$, while the threshold ϕ_* represents a maximum packing density. The function $\mathscr{P}$ is intended to account for the mechanical stress exerted by the surrounding cells in a population of tumor cells: the higher the density, the higher the stress. The stress induces a motion of the cell, see [15, 43, 44], with a velocity proportional to the pressure gradient, in the spirit of Darcy's law. As the exponent ν increases, the effect of the threshold becomes more sensitive, since gradients are very stiff for densities above the threshold. Therefore, the regime $\nu \to \infty$ makes a connection with models describing tumor growth by means of free boundary problems [23, 45], where the tumor is described as a moving domain of constant density. For the tumor cells, the source terms account for the proliferation/necrosis of the cells, as well as for the action of the immune cells. Proliferation/necrosis are driven by the availability of nutrient and the homeostatic pressure, while antitumor immune cells kill tumor cells and protumor cells enhance the proliferation. Moreover, cell proliferation is governed by a biomechanical form of contact inhibition, that prevents cell division when the total cell density exceeds a critical threshold. This effect is accounted for again by using the function $\mathscr{P}$, [15, 23, 45]. We thus get

$$\Gamma_n = \frac{\rho_n \phi_n}{\tau_n}(\Upsilon(\mathscr{P}, O, \phi_p) - A_a \phi_a).$$

In this expression O stands for the oxygen and nutrient concentration, τ_n can be interpreted as a relaxation time and A_a describes the strength of the antitumor immune cells on tumor cells. The coupling function Υ fulfils the following assumptions

$$\partial_{\mathscr{P}}\Upsilon < 0, \qquad \partial_O \Upsilon \geq 0, \qquad \partial_{\phi_p}\Upsilon \geq 0.$$

Proliferation is indeed more effective when the pressure is low and nutrient availability is high; it is enhanced under the action of protumor immune cells.

It might be relevant to assume that Υ vanishes when $O \in [O_*, O^*]$ (quiescent phase) and $\Upsilon < 0$ when $O \in [0, O_*[$: when the oxygen concentration falls below the critical threshold O_*, then the tumor cells are unable to survive and undergo necrotic cell death. In the latter case, Υ does not correspond to a gain term and, for further purposes, it is convenient to decompose $\Upsilon = [\Upsilon]_+ - [\Upsilon]_-$, with $[\Upsilon]_\pm = \max(0, \pm\Upsilon) \geq 0$). A possible expression, inspired from the standard logistic law, leads to

$$\Gamma_n = \frac{\rho_n \phi_n}{\tau_n} \left(k_{+O}[O - O^*]_+ (1 + \phi_p) - \left(k_{-O}[O - O_*]_- + \frac{\mathscr{P}}{p_*} \right) - A_a \phi_a \right),$$

with $k_{\pm O} > 0$ appropriate dimensionalizing constants. Quite similar coupling accounting for close-packing effects, and coupling with oxygen/nutriments supply can be found in [11, Eq. (15)]. As far as we know, there is no established model for the expression of the source term Γ_n, beyond the natural monotonicity properties stated above. For $\phi_a = \phi_p = 0$, $O > O^*$, the proposed formula behaves like the logistic law. It also combines several mechanisms, considered as independent, that lead to the elimination of tumor cells: the action of immune cells (ϕ_a), the lack of oxygen-nutrients ($O < O_*$), and the compression effects that restrict the tumor development [15]. As we shall see below, the pressure term $\mathscr{P}$ can be significant only when the tumor volume fraction approaches a threshold (see (10) with $\nu \gg 1$); however, even when the tumor volume fraction is small, the lack of oxygen leads to the necrosis of the tumor cells.

2.1.3. Mass exchange for the environment

Loss terms for the other constituents become gain terms for the environment, while the protumor reactions, in particular through CAF and MMP enzymes, promote the degradation of the environment. We otherwise consider that healthy cells are not dividing relatively to the proliferative cells and that they do not die from environmental conditions (or, maybe more appropriately, that the two effects balance). We are thus led to

$$\Gamma_m = \gamma_a \rho_a \phi_a + \gamma_p \rho_p \phi_p + \frac{\rho_a \phi_a \phi_p}{\tau_{ap}} + \frac{\rho_n}{\tau_n} \phi_n \phi_a + \frac{\rho_n}{\tau_n} \phi_n [\Upsilon]_- - \rho_m \phi_m f(I).$$

The function $f : [0, \infty) \to [0, \infty)$ describes the degradation of the healthy environment by the action of cytokines and CAF; possible expressions are $f(I) = f_* I$ or $f(I) = \frac{f_* I}{1 + I/I_*}$ in order to take into account some limitation mechanisms. (For the simulations we only use the linear law.)

We remark that the total mass balance is given by

$$\Gamma_a + \Gamma_p + \Gamma_n + \Gamma_m = \rho_a g(\mu_n) S_a + k_{Ip} I \rho_p S_p + \frac{\rho_n}{\tau_n} \phi_n [\Upsilon]_+ - \rho_m \phi_m f(I).$$

The total mass increases due to the tumor proliferation and the sources of anti- and protumor cells; it decreases due to the degradation of the environment. In particular if the source of immune cells vanish ($S_p = S_a = 0$), if there are no cytokines degrading the environment ($I = 0$) and no supply of nutrient ($O < O^*$ implies $[\Upsilon]_+ = 0$), then the mass balance vanishes. Another quantity of interest is the total volume balance

$$\begin{aligned}
&\frac{\Gamma_a}{\rho_a} + \frac{\Gamma_p}{\rho_p} + \frac{\Gamma_n}{\rho_n} + \frac{\Gamma_m}{\rho_m} \\
&= \Big(g(\mu_n) S_a - \phi_a \big(\gamma_a + k_{Ia} I + \frac{\phi_p}{\tau_{ap}} \big) \Big) \\
&\qquad + k_{Ip} I S_p + \frac{\rho_a}{\rho_p} \phi_a k_{Ia} I - \gamma_p \phi_p + \frac{\phi_n}{\tau_n} (\Upsilon(\mathscr{P}, O, \phi_p) - A_a \phi_a) \\
&\qquad + \gamma_a \frac{\rho_a}{\rho_m} \phi_a + \gamma_p \frac{\rho_p}{\rho_m} \phi_p + \frac{\rho_a}{\tau_{ap} \rho_m} \phi_a \phi_p + \frac{\rho_n}{\tau_n \rho_m} \phi_n \phi_a + \frac{\rho_n}{\tau_n \rho_m} \phi_n [\Upsilon]_- - \phi_m f(I) \\
&\neq 0
\end{aligned}$$

which could be non-zero, even when the mass balance vanishes. In [21, 46] such a non zero volume contribution appear. This quantity is involved in the boundary condition through (5).

2.2. Oxygen and nutrient

Concentrations of oxygen and nutrients are diffused rapidly: we apply the adiabatic approximation which assumes that the diffusion process occurs on much smaller time scales that the cell motion and divisions [13, 19, 43]. Therefore we suppose that the equilibrium is reached instantaneously: the concentration O satisfies the Poisson equation

$$\nabla_x \cdot (O \chi_O \nabla_x \phi_n) - \nabla_x \cdot (D_O \nabla_x O) = S_O - O(r_n \rho_n \phi_n + r_a \rho_a \phi_a + r_p \rho_p \phi_p + r_m \rho_m \phi_m). \tag{11}$$

This equation incorporates a drift term directed towards higher gradients of the tumor volume fraction, with a chemotactic coefficient χ_O which can be defined as a function of ϕ_n, typically with a sigmoidal shape. The right hand side describes the consumption of nutrient from a given source S_O, say strongly located next to the vessels. It involves rates r_j that can differ depending on the considered component. In particular, the consumption rate

of the tumor r_n can be substantially greater than the other rates r_a, r_p, r_m (Warburg effect), [36]. The equation is endowed with a (possibly non homogeneous) Dirichlet boundary condition.

The critical role of the access to nutrients and oxygen in sustaining tumor's development has been reported in many experiments [2, 17]. This should be reflected in the coupling between (11) and the proliferation/necrosis terms in the mass balance equation for the tumor, as described in Section 2.1.2. To proliferate, cells need nutrient and oxygen coming from existing vascular vessels surrounding the tissue where the tumor grows. As the tumor develops, in regions of high volume fraction, tumor cells are progressively starved of oxygen and nutrient (locally the oxygen concentration falls below the threshold O^* due to the consumption by a large number of tumor cells) and, in consequence, their proliferation rate and the tumor's overall growth rate decline (see the definition of Υ in Section 2.1.2). However, starving cells have the ability to secrete factors and chemoattractants in order to induce the formation of new blood vessels towards the tumor. This is called the process of angiogenesis, which can be roughly taken into account through the coefficient χ_O in (11). Note also that a more complicated consumption term for the tumor can be considered as well, replacing $r_n\rho_n\phi_n$ by a function U which can depend on the homeostatic pressure $\mathscr{P}$ and O such that $\partial_{\mathscr{P}}U \leq 0$, $\partial_{\mathscr{O}}U \geq 0$, $U(\mathscr{P}, 0) = 0$, see [23, 45]. Moreover, immune cells, once activated, have also a substantial demand in oxygen and nutrients and the competition for the resources is also a key factor in the efficacy of the immune response [36]. Note that, here, we neglect the effect of oxygen availability on the immune cells; however the consumption due to the immune cells impacts the resources remaining for the tumor development.

2.3. Momentum fluxes

There is a huge variety of closure relations for defining the mass fluxes (2). According to [49], and the applications of mixture theory for cancer growth modeling [3, 11, 14, 17, 35, 47, 48], or biofilm formation [46], we follow a mechanical approach: we consider momentum equations satisfied by the velocities V_j, with force terms depending on each phase. The latter incorporate chemotactic effects, homeostatic pressure and drag forces. The momentum equations have the general formulation

$$\frac{\partial}{\partial t}\left(\rho_j\phi_j V_j\right) + \operatorname{div}\left(\rho_j\phi_j V_j \otimes V_j\right) = \operatorname{div}(\sigma_j) + \mathcal{F}_j$$

Neglecting convective effects in the left hand side, the equations reduce to

$$-\mathrm{div}(\sigma_j) = \mathcal{F}_j$$

with σ_j the stress tensor, and $\mathcal{F}_j$ the applied force. All constituents are subjected to a common "hydrostatic" pressure Π, which can be interpreted as the Lagrange multiplier associated to the constraint (3), the analog of the usual pressure field for solenoidal flows. Then, we split the stress tensor into several contributions

$$\sigma_j = -\rho_j\phi_j\Pi\mathbb{I} - \rho_j\phi_j\mathcal{P}_j\mathbb{I} + \frac{\varpi_j}{2}(\nabla V_j + \nabla V_j^\intercal).$$

In the last two terms, we recognize:

- the viscous term, where the dynamic viscosity ϖ_j is supposed to be constant,
- an additional, isotropic, pressure field $\mathcal{P}_j$ which is specific to the considered phase [11, 14, 35, 46], taking into account interactions between cells of the same constituent. We adopt the following definition:
  - tumor cells are sensitive to close-packing effects: as the tumor volume fraction increases, tumor cell membrane deforms, inducing a stress. This is described by the homeostatic pressure term $\mathscr{P}$, which becomes large as the tumor volume fraction approaches the threshold ϕ_* [14].
  - the presence of immune cells induces a compression effect, which is assumed to grow linearly with the volume fraction: $\mathcal{P}_a = D_a$, $\mathcal{P}_p = D_p$, with $D_a, D_p > 0$, [35, 46].
  - the environment is considered as a carrying fluid, and does not support additional pressure $\mathcal{P}_m = 0$.

We turn to the description of the forces:

- the motion of immune cells is driven by chemotaxis, defined through a common potential Φ, activated by the tumor. We have

$$-\nabla_x \cdot (D_\Phi \nabla_x \Phi) = \rho_n\Big(\phi_n - \frac{1}{|\Omega|}\int \phi_n \,\mathrm{d}x\Big), \tag{12}$$

  endowed with Neumann boundary conditions. The chemotactic coefficients χ_a, χ_p are positive constants with the appropriate dimension.

- the constituent labelled by j is subjected to drag forces exerted by the other constituents

$$drag_j = \rho_j \phi_j \sum_{\ell \neq j} \lambda_{j\ell} \phi_\ell (V_\ell - V_j),$$

  where the coefficients $\lambda_{j\ell}$ are homogeneous to the inverse of a time.

- the co-occupancy of the domain by several constituents induce interfacial forces, orthogonal to the level curve of the volume fraction, namely $\rho_j \Pi \nabla \phi_j$.

- the momentum supply associated to the mass exchanges $\Gamma_j V_j$.

Summing up these contributions yields

$$\mathcal{F}_j = \Gamma_j V_j + drag_j + \rho_j \Pi \nabla \phi_j + \rho_a \phi_a \chi_a \nabla_x \Phi + \rho_p \phi_p \chi_p \nabla_x \Phi.$$

By using the identity $\mathrm{div}(\phi_j \Pi \mathbb{I}) = \nabla(\phi_j \Pi) = \Pi \nabla \phi_j + \phi_j \nabla \Pi$, we arrive at

$$\begin{aligned} -\varpi_j \Delta_x V_j + \rho_j \phi_j \nabla_x \Pi + \rho_j \Pi \nabla_x \phi_j + \rho_j \phi_j \nabla_x \mathcal{P}_j + \rho_j \mathcal{P}_j \nabla_x \phi_j = \Gamma_j V_j + drag_j \\ + \rho_j \Pi \nabla_x \phi_j + \rho_a \phi_a \chi_a \nabla_x \Phi + \rho_p \phi_p \chi_p \nabla_x \Phi, \end{aligned}$$

and then

$$-\varpi_j \Delta_x V_j + \rho_j \phi_j \nabla_x \Pi = \Gamma_j V_j + drag_j + F_j,$$

where all terms in this relation are homogeneous to $\frac{mass}{length^2 time^2}$. In this momentum balance, the force terms are given by

$$\begin{aligned} F_n &= -\rho_n \nabla_x (\phi_n \mathscr{P}), & F_m &= 0, \\ F_a &= \rho_a (\phi_a \chi_a \nabla_x \Phi - D_a \nabla_x \phi_a), & F_p &= \rho_p (\phi_p \chi_p \nabla_x \Phi - D_p \nabla_x \phi_p). \end{aligned}$$

The model can be simplified by

- neglecting all drag terms but with the environment,

- neglecting a part or all the viscous terms so that momentum equations reduce to force balance [19, 35],

- neglecting the contribution of the momentum associated to the mass exchanges [47].

Based on such assumptions (with $\varpi_a, \varpi_p, \varpi_n \ll \varpi_m$) we get

- For the tumor

$$\rho_n\phi_n\phi_m\lambda_{nm}(V_m - V_n) - \rho_n\nabla_x(\phi_n\mathscr{P}) = \rho_n\phi_n\nabla_x\Pi,$$

- For the antitumor immune cells

$$\rho_a\phi_a\phi_m\lambda_{am}(V_m - V_a) + \rho_a(\phi_a\chi_a\nabla_x\Phi - D_a\nabla_x\phi_a) = \rho_a\phi_a\nabla_x\Pi,$$

- For the protumor immune cells

$$\rho_p\phi_p\phi_m\lambda_{pm}(V_m - V_p) + \rho_p(\phi_p\chi_p\nabla_x\Phi - D_p\nabla_x\phi_p) = \rho_p\phi_p\nabla_x\Pi,$$

- For the environment

$$-\varpi_m\Delta_x V_m + \rho_m\phi_m\nabla_x\Pi = \rho_m\phi_m(\phi_n\lambda_{nm}(V_n - V_m) + \phi_a\lambda_{am}(V_a - V_m) + \phi_p\lambda_{pm}(V_p - V_m)).$$

We divide by the mass densities and we sum up to obtain

$$-\frac{\varpi_m}{\rho_m}\Delta_x V_m + \nabla_x\Pi = -\nabla_x(\phi_n\mathscr{P}) + (\phi_a\chi_a\nabla_x\Phi - D_a\nabla_x\phi_a) + (\phi_p\chi_p\nabla_x\Phi - D_p\nabla_x\phi_p),$$

and the other velocities are deduced form (V_m, Π) by

$$\begin{aligned}
V_n &= V_m - \frac{1}{\phi_m\lambda_{nm}}(\nabla_x\Pi + \nabla_x(\phi_n\mathscr{P})),\\
V_a &= V_m - \frac{1}{\phi_m\lambda_{am}}\Big(\nabla_x\Pi - \chi_a\nabla_x\Phi + \frac{D_a}{\phi_a}\nabla_x\phi_a\Big),\\
V_p &= V_m - \frac{1}{\phi_m\lambda_{pm}}\Big(\nabla_x\Pi - \chi_p\nabla_x\Phi + \frac{D_p}{\phi_p}\nabla_x\phi_p\Big).
\end{aligned}$$

In other words, the mass fluxes read

$$\begin{aligned}
\mathscr{J}_n &= \rho_n\phi_n\Big(V_m - \frac{1}{\phi_m\lambda_{nm}}\nabla_x\Pi\Big) - \frac{\rho_n}{\phi_m\lambda_{nm}}\nabla_x(\phi_n\mathscr{P})\\
\mathscr{J}_a &= \rho_a\phi_a\Big(V_m - \frac{1}{\phi_m\lambda_{am}}(\nabla_x\Pi - \chi_a\nabla_x\Phi)\Big) - \frac{\rho_a}{\phi_m\lambda_{am}}D_a\nabla_x\phi_a,\\
\mathscr{J}_p &= \rho_p\phi_p\Big(V_m - \frac{1}{\phi_m\lambda_{pm}}(\nabla_x\Pi - \chi_p\nabla_x\Phi)\Big) - \frac{\rho_p}{\phi_m\lambda_{pm}}D_p\nabla_x\phi_p,
\end{aligned}$$

which make convection and diffusion effects appear. In particular, it can be convenient to rewrite the homeostatic pressure gradient as follows

$$\nabla_x(\phi_n\mathscr{P}) = (\mathscr{P}(\phi_n) + \phi_n\mathscr{P}'(\phi_n))\nabla_x\phi_n = \nabla_x\mathscr{Q}(\phi_n), \quad \mathscr{Q}'(z) = z\mathscr{P}'(z) + \mathscr{P}(z).$$

The system is closed by coming back to the saturation constraint (4) which becomes

$$\begin{aligned}\nabla_x \cdot (\phi_n V_n + \phi_a V_a + \phi_p V_p + \phi_m V_m) &= \frac{\Gamma_a}{\rho_a} + \frac{\Gamma_p}{\rho_p} + \frac{\Gamma_n}{\rho_n} + \frac{\Gamma_m}{\rho_m} \\ = \nabla_x \cdot \Big(V_m - \Big(\frac{\phi_n}{\phi_m \lambda_{nm}} + \frac{\phi_a}{\phi_m \lambda_{am}} + \frac{\phi_p}{\phi_m \lambda_{pm}} \Big) \nabla_x \Pi - \frac{\nabla_x(\phi_n \mathscr{P})}{\phi_m \lambda_{nm}} \\ + \Big(\frac{\phi_a \chi_a}{\phi_m \lambda_{am}} + \frac{\phi_p \chi_p}{\phi_m \lambda_{pm}} \Big) \nabla_x \Phi - \frac{D_a}{\phi_m \lambda_{am}} \nabla_x \phi_a - \frac{D_p}{\phi_m \lambda_{pm}} \nabla_x \phi_p \Big) .\end{aligned}$$

Note the structure of the Stokes-like equation for (V_m, Π)

$$\begin{pmatrix} -\frac{\varpi_m}{\rho_m} \Delta_x & \nabla_x \\ \nabla_x \cdot & -\nabla_x \cdot (\alpha \nabla_x) \end{pmatrix} \begin{pmatrix} V_m \\ \Pi \end{pmatrix} = RHS$$

with α positively valued. As for the usual Stokes problem, the pressure is defined up to a constant. Accordingly, when multiplying the LHS by (V_m, Π), we get (neglecting boundary terms)

$$\begin{aligned}&\frac{\varpi_m}{\rho_m} \int |\nabla V_m|^2 \, \mathrm{d}x - \int \Pi \nabla_x \cdot V_m \, \mathrm{d}x + \int \nabla_x \cdot V_m \Pi \, \mathrm{d}x + \int \alpha |\nabla_x \Pi|^2 \, \mathrm{d}x \\ &= \frac{\varpi_m}{\rho_m} \int |\nabla V_m|^2 \, \mathrm{d}x + \int \alpha |\nabla_x \Pi|^2 \, \mathrm{d}x\end{aligned}$$

which is a good indication for well posedness of the linearized problem. We also remark that the healthy state $\phi_m = 1$, $\phi_a = \phi_p = \phi_n = 0$ with (V_m, Π) solution of the standard Stokes equation is solution of the system.

2.4. Boundary conditions

We expect that the tumor, and thus the anti- and protumor activities, are located far from the boundaries of the domain and do not substantially interact with the external domains. Bearing in mind the convection-diffusion nature of the corresponding mass fluxes, it thus makes sense to assume

- either the homogeneous Dirichlet boundary conditions for these volume fractions:
$$\phi_n, \ \phi_a, \ \phi_p \big|_{\partial\Omega} = 0. \tag{13}$$
- or the zero-flux conditions
$$(\mathscr{J}_n, \ \mathscr{J}_a, \ \mathscr{J}_p) \cdot \nu_x \big|_{\partial\Omega} = 0. \tag{14}$$

It is also possible to mix these conditions, depending on the considered type of cells. The Dirichlet condition (13) is certainly relevant for the tumor cells, which can be supposed located far from the boundaries of the computational domain, but it might be questionable for the immune cells: biologically, the spatial distribution of the source of immune cells and the boundary conditions can be related to the type of cytotoxic cells considered in the modeling. Indeed, the immune response combines different type of cells, typically NK cells and T cells, which here are all considered as making a single species, described by the volume fraction ϕ_a (and ϕ_p). On the one hand, NK cells are patrolling in the body, their source could be assumed to be homogeneously distributed and (14) makes sense for such cells. On the other hand, T cells need to be activated by an efficient priming process which occurs in the draining lymph nodes; their sources are therefore non-homogeneously distributed and (13) is relevant for such cells, meaning that the immune cells far from the tumor are in their naive state. We refer the reader to [6] for further comment on the influence of the space organization of the sources of immune cells. We made computations with the two types of boundary conditions and the presented conclusions are not substantially impacted by the choice of the boundary condition for the immune cells.

The boundary conditions for ϕ_m and V_m are more intricate and should be consistent with (5). We distinguish the design of the boundary condition, depending whether we use (13) or (14). Assuming (13), we can impose that the tangential velocity vanishes

$$V_m \cdot \tau_x\big|_{\partial\Omega} = 0,$$

and for the normal coordinates, we remind the reader that

$$\begin{aligned}
&(\phi_n V_n + \phi_a V_a + \phi_p V_p + \phi_m V_m) \cdot \nu_x \\
&= V_m \cdot \nu_x - \Big(\frac{\phi_n}{\phi_m \lambda_{nm}} + \frac{\phi_a}{\phi_m \lambda_{am}} + \frac{\phi_p}{\phi_m \lambda_{pm}}\Big) \nabla_x \Pi \cdot \nu_x - \frac{1}{\phi_m \lambda_{nm}} \nabla_x (\phi_n \mathscr{P}) \cdot \nu_x \\
&\qquad + \Big(\frac{\phi_a \chi_a}{\phi_m \lambda_{am}} + \frac{\phi_p \chi_p}{\phi_m \lambda_{pm}}\Big) \nabla_x \Phi \cdot \nu_x - \frac{D_a}{\phi_m \lambda_{am}} \nabla_x \phi_a \cdot \nu_x - \frac{D_p}{\phi_m \lambda_{pm}} \nabla_x \phi_p \cdot \nu_x \\
&= V_m \cdot \nu_x - \frac{1}{\phi_m} \left(\frac{1}{\lambda_{nm}} \nabla_x \mathscr{Q} + \frac{D_a}{\lambda_{am}} \nabla_x \phi_a + \frac{D_p}{\lambda_{pm}} \nabla_x \phi_p \right) \cdot \nu_x
\end{aligned}$$

where

$$\mathscr{Q}'(z) = z\mathscr{P}'(z) + \mathscr{P}(z).$$

Bearing in mind that $\phi_m = 1 - \phi_a - \phi_p - \phi_n = 1$ on $\partial\Omega$ due to (13), we thus decide to impose on $\partial\Omega$

$$V_m \cdot \nu_x = \Big(\frac{1}{\lambda_{nm}}\nabla_x \mathscr{Q} + \frac{D_a}{\lambda_{am}}\nabla_x \phi_a + \frac{D_p}{\lambda_{pm}}\nabla_x \phi_p\Big)\cdot \nu_x + \frac{1}{|\partial\Omega|}\int_\Omega \Big(\frac{\Gamma_a}{\rho_a} + \frac{\Gamma_p}{\rho_p} + \frac{\Gamma_n}{\rho_n} + \frac{\Gamma_m}{\rho_m}\Big)\,\mathrm{d}x. \tag{15}$$

Assuming (14), we can use the following definition for the normal and tangential components of the velocity field V_m

$$\begin{aligned} &V_m \cdot \nu_x\big|_{\partial\Omega} = \frac{1}{|\partial\Omega|}\int_\Omega \Big(\frac{\Gamma_a}{\rho_a} + \frac{\Gamma_p}{\rho_p} + \frac{\Gamma_n}{\rho_n} + \frac{\Gamma_m}{\rho_m}\Big)\,\mathrm{d}x, \\ &V_m \cdot \tau_x\big|_{\partial\Omega} = 0. \end{aligned} \tag{16}$$

Namely, we impose the constant flux which is compatible with the relation (5).

2.5. One dimensional case

In order to guide the intuition and to assess the qualitative properties of the model, we shall perform a series of numerical simulations, restricting ourselves to the one-dimensional framework. Let us collect the equations in this specific context. The unknowns are the volume fractions $\phi_n, \phi_a, \phi_p, \phi_m$, the concentrations O, I, the chemotactic potential Φ, the velocity field V_m and the hydrostatic pressure Π.

The mass balance equations for $\phi_n, \phi_a, \phi_p, \phi_m$ read

$$\begin{aligned} &\partial_t(\rho_n\phi_n) + \partial_x\Big(\rho_n\phi_n\Big(V_m - \frac{\partial_x\Pi}{\lambda_{nm}\phi_m}\Big)\Big) - \partial_x\Big(\frac{\rho_n \mathscr{Q}'(\phi_n)}{\lambda_{nm}\phi_m}\partial_x\phi_n\Big) \\ &\qquad = \frac{\rho_n\phi_n}{\tau_n}(\Upsilon(\mathscr{P}, O, \phi_p) - A_a\phi_a), \\ &\partial_t(\rho_a\phi_a) + \partial_x\Big(\rho_a\phi_a\Big(V_m - \frac{\partial_x\Pi}{\lambda_{am}\phi_m} + \frac{\chi_a}{\lambda_{am}\phi_m}\partial_x\Phi\Big)\Big) - \partial_x\Big(\frac{\rho_a D_a}{\lambda_{am}\phi_m}\partial_x\phi_a\Big) \\ &\qquad = \rho_a g\left(\int \rho_n\phi_n\,\mathrm{d}x\right)S_a - \rho_a\phi_a\Big(\gamma_a + k_{Ia}I + \frac{\phi_p}{\tau_{ap}}\Big), \\ &\partial_t(\rho_p\phi_p) + \partial_x\Big(\rho_p\phi_p\Big(V_m - \frac{\partial_x\Pi}{\lambda_{pm}\phi_m} + \frac{\chi_p}{\lambda_{pm}\phi_m}\partial_x\Phi\Big)\Big) - \partial_x\Big(\frac{\rho_p D_p}{\lambda_{pm}\phi_m}\partial_x\phi_p\Big) \\ &\qquad = k_{Ip}I\rho_p S_p + \rho_a\phi_a k_{Ia}I - \gamma_p\rho_p\phi_p, \\ &\partial_t(\rho_m\phi_m) + \partial_x(\rho_m\phi_m V_m) \\ &\qquad = \gamma_a\rho_a\phi_a + \gamma_p\rho_p\phi_p + \frac{\rho_a\phi_a\phi_p}{\tau_{ap}} + \frac{\rho_n}{\tau_n}\phi_n\phi_a + \frac{\rho_n}{\tau_n}\phi_n[\Upsilon]_- - \rho_m\phi_m f(I), \end{aligned} \tag{**Full)**}$$

together with the constraint

$$\phi_n + \phi_a + \phi_p + \phi_m = 1.$$

Here, we set

$$\Upsilon(\mathscr{P}, O, \phi_p) = k_{+O}[O - O^*]_+(1 + \phi_p) - \Big(k_{-O}[O - O_*]_- + \frac{\mathscr{P}}{p_*}\Big).$$

This set of equations will be referred to as the "Full" model, in contrast with reduced models where some effects and couplings will be neglected. The equations for the oxygen-nutrient concentration, chemotaxis potential, and protumor cytokine signal read

$$\begin{aligned}
&\partial_x\left(O\chi_O\partial_x\phi_n\right) - \partial_x(D_O\partial_x O) = S_O - O(r_n\rho_n\phi_n + r_a\rho_a\phi_a + r_p\rho_p\phi_p + r_m\rho_m\phi_m)\\
&O\big|_{x=0,L} = O_{bd},\\
&-\partial_x(D_\Phi\partial_x\Phi) = \rho_n\Big(\phi_n - \frac{1}{|\Omega|}\int \phi_n\,\mathrm{d}x\Big),\\
&\partial_x\Phi\big|_{x=0,L} = 0,\\
&\frac{\mathrm{d}}{\mathrm{d}t}I = \psi(\phi_n, \phi_m) - \frac{I}{\tau}.
\end{aligned} \tag{17}$$

Finally, the velocity V_m and pressure Π satisfy

$$\begin{aligned}
&-\frac{\varpi_m}{\rho_m}\partial_{xx}^2 V_m + \partial_x\Pi = -\partial_x(\phi_n\mathscr{P}) + (\phi_a\chi_a\partial_x\Phi - D_a\partial_x\phi_a) + (\phi_p\chi_p\partial_x\Phi - D_p\partial_x\phi_p),\\
&\partial_x\Bigg(V_m - \Big(\frac{\phi_n}{\phi_m\lambda_{nm}} + \frac{\phi_a}{\phi_m\lambda_{am}} + \frac{\phi_p}{\phi_m\lambda_{pm}}\Big)\partial_x\Pi - \frac{1}{\phi_m\lambda_{nm}}\partial_x(\phi_n\mathscr{P})\\
&\qquad + \Big(\frac{\phi_a\chi_a}{\phi_m\lambda_{am}} + \frac{\phi_p\chi_p}{\phi_m\lambda_{pm}}\Big)\partial_x\Phi - \frac{D_a}{\phi_m\lambda_{am}}\partial_x\phi_a - \frac{D_p}{\phi_m\lambda_{pm}}\partial_x\phi_p\Bigg)\\
&\qquad = \frac{\Gamma_a}{\rho_a} + \frac{\Gamma_p}{\rho_p} + \frac{\Gamma_n}{\rho_n} + \frac{\Gamma_m}{\rho_m}.
\end{aligned} \tag{18}$$

The system is completed with the following boundary conditions: we impose the Dirichlet conditions

$$\phi_a, \phi_p, \phi_n\big|_{x=0,L} = 0, \qquad \phi_m\big|_{x=0,L} = 1,$$

together with

$$V_m\nu_x\big|_{x=0,L} = + \int_0^L \Big(\frac{\Gamma_a}{\rho_a} + \frac{\Gamma_p}{\rho_p} + \frac{\Gamma_n}{\rho_n} + \frac{\Gamma_m}{\rho_m}\Big)\,\mathrm{d}x$$

(with the convention $\nu_0 = -1$, $\nu_L = +1$).

3. Numerical investigations: reduced models and role of the parameters

We are going to investigate numerically the proposed system of equations. It is worthwhile to make a hierarchy of models appear, with the freedom to disregard a part of the phenomena. The interest of this approach is two-fold. On the one hand, these reduced equations can be relevant for describing different stages of the tumor evolution. On the other hand, it will permit us to discuss more clearly the role and influence of the different modeling assumptions.

The numerical treatment of such a complicated system of partial differential equations raises several delicate issues. In particular, one should pay attention to preserve the positivity of the volume fractions and concentrations, which requires to identify suitable stability conditions. Next, the constraint (3) has several formulations and consequences, which are not obviously conserved when discretizing the equations. Finally, the Stokes-like system for the pair (V_m, Π) has a structure which deserves a specific treatment. These issues will be analyzed elsewhere [51]; they definitely require the design of a dedicated scheme, see also the attempt in [9].

For the simulations, we restrict to the one-dimensional framework: the computational domain is the slab $[-1.5, 1.5]$. Table 1 collects the definition of the unknowns. Otherwise explicitly stated, the simulations are performed with the parameters collected in Table 2. We start with a small tumor located at the center of the computational domain, namely the initial volume fraction of tumor cells is given by

$$\phi_n(0, x) = 0.1 \times \exp^{-40x^2}. \tag{19}$$

The numerical parameters have been chosen so that positivity of the unknowns and numerical convergence have been fairly observed; namely we have set $\delta t = 10^{-3}$, $h = 0.015$.

Focusing on the one dimensional framework is only a step towards more ambitious and realistic simulations. The advantage is to have a simple framework, where the code development is not too demanding and many simulations are affordable, in order to push forward the analysis of the behavior of the model and the role of the parameters. This is a preliminary, but essential, step before working on 2D or starting a sensitivity analysis concentrated on a few key parameters. Similarly, we assign quite arbitrary and academic

Variable	Description
ϕ_n	volume fraction of tumor cells
ϕ_a	volume fraction of antitumor immune cells
ϕ_p	volume fraction of protumor immune cells
ϕ_m	volume fraction of the environment
I	cytokine concentration
O	concentration of oxygen/nutrient
Φ	chemotactic potential for immune cells

Table 1: Definition of the unknowns

values of the parameters, which are often not accessible to experiments[3]: our goal here is rather to assess qualitatively their relative influence, more than claiming quantitative conclusions. The parameters are chosen in order to explore on numerical grounds the consequences of the modeling assumptions and to identify what are the main drivers of the tumor growth, and what effects could be activated to boost efficiently the immune response.

We are going to discuss reduced models of variable complexity in order to clarify on numerical grounds the role of the modeling assumptions and parameters. In order to ease the identification of the tested models, we shall use acronyms, recapped in Table 3:

- The **(T)** model neglects all interactions and consists in a mere scalar diffusion-reaction equation for the tumor cells. We will discuss the influence of the exponent ν in the homeostatic pressure law in shaping propagation fronts.

- The **(T.A.)** model restricts to the coupling between the tumor and the antitumor immune response, in a given environment.

- The **(T.E.O.)** model focuses on the interaction between the tumor and the environment, accounting for the oxygen and nutrient supply. In particular, we discuss how the necrotic/proliferation thresholds, the localization of the oxygen and nutrient sources and the attracting capabilities of the tumor cells shape the tumor development.

[3]An important difficulty relies on the lack of the time evolution of the data on the TME, for a given individual, which makes identification methods inoperative

Variable	Description	Value
$\phi_n(0,x)$	initial condition for the volume fraction of tumor cells	Eq. (19)
$\phi_a(0,x)$	initial condition for the volume fraction of antitumor immune cells	0
$\phi_p(0,x)$	initial condition for the volume fraction of protumor immune cells	0
$I(0,x)$	initial condition for the cytokine concentration	0
ρ_n	mass density of tumor cells	1
ρ_a	mass density of antitumor immune cells	1
ρ_p	mass density of protumor immune cells	1
ρ_m	mass density of the environment	1
p_*	reference (homeostatic) pressure	1
ϕ_*	threshold for the tumor volume fraction (maximum packing density)	.7
ν	exponent for the packing (homeostatic) pressure	5–50
D_a	diffusion coefficient of antitumor immune cells	1/40
D_p	diffusion coefficient of protumor immune cells	1/40
D_Φ	diffusion coefficient of the chemotactic signal	1
D_O	diffusion coefficient of the oxygen/nutrient	.5
χ_a	chemotactic coefficient of antitumor immune cells	.864
χ_p	chemotactic coefficient of protumor immune cells	.864
χ_O	chemotactic coefficient of oxygen concentration	1
γ_a	death rate of the antitumor immune cells	.18
γ_p	death rate of the protumor immune cells	.2
A_a	strength of the antitumor immune cells on tumor cells	5
S_a	source of antitumor immune cells	3
S_p	source of protumor immune cells	3
S_O	source of oxygen/nutrient	(20a)-(20c)
g_0	activation rate of effector immune cells	1
O_*	hypoxia threshold for the oxygen concentration	.1
O^*	tumor proliferation threshold for the oxygen concentration	.3
k_{+O}	appropriate dimensionalizing constant of oxygen concentration	1
k_{-O}	appropriate dimensionalizing constant of oxygen concentration	1
r_n	consumption rate of oxygen/nutrient by tumor cells	.3
r_a	consumption rate of oxygen/nutrient by antitumor immune cells	.1
r_p	consumption rate of oxygen/nutrient by protumor immune cells	.1
r_m	consumption rate of oxygen/nutrient by the environment	.1
f_*	enhanced environment degradation rate due to CAF and cytokines	0-1
$\phi_{n_{I,s}}$	threshold related to the tumor volume fraction for cytokine production	0
$\phi_{m_{I,s}}$	threshold related to the environment volume fraction for cytokine production	0
k_{Ia}	conversion rate of antitumor immune cells into protumor cells	1
k_{Ip}	rate of activation of naive cells into protumor immune cells by cytokines	1
τ_n	relaxation time for tumor cells	1
τ_{ap}	relaxation time of the annihilation of antitumor immune cells by the protumor immune cells	1
τ	relaxation time for cytokines	1
λ_{nm}	drag coefficient between tumor cells and the environment	1
λ_{am}	drag coefficient between antitumor immune cells and the environment	1
λ_{pm}	drag coefficient between protumor immune cells and the environment	1
ϖ_m	dynamic viscosity of the environment	.1

Table 2: Definitions and values of the parameters used for the simulations

- The **(T.A.E.O.)** model couples the tumor growth, the antitumor immune response, and the environment, showing how the competition for space and resources organizes the TME.
- The **(Full)** model that additionally incorporates the protumor immune cells and their actions promoting the tumor growth.

Models	Description
(T)	Tumor growth model
(T.A.)	Tumor-antitumor immune cells model
(T.E.O.)	Tumor-Environment and Oxygen model
(T.A.E.O.)	Tumor-antitumor immune cells-Environment and Oxygen model
(Full)	Tumor-anti and protumor immune cells-Environment and Oxygen model

Table 3: Reduced models

*3.1. Evolution of an immune-free small tumor volume fraction (model **(T)**)*

The simplest situation is obtained by completely neglecting the immune response, which means imposing $\phi_a = \phi_p = 0$. Moreover, we suppose that the tumor volume fraction is very small $\phi_n \ll \phi_m \simeq 1$. It turn, the velocity-pressure pair (V_m, Π) can be assumed to satisfy the free Stokes equation, which yields $V_m = 0$ and Π is constant. This set of assumptions might correspond to the earliest stages of the tumor growth. In this regime we also neglect the influence of the nutrient supply: it is supposed to be constant, space homogeneous and sufficient to sustain tumor proliferation. The model then reduces to a mere scalar equation

$$\partial_t(\rho_n\phi_n) - \partial_x\Big(\frac{\rho_n\mathscr{Q}'(\phi_n)}{\lambda_{nm}(1-\phi_n)}\partial_x\phi_n\Big) = \frac{\rho_n\phi_n}{\tau_n}\Upsilon(\mathscr{P}), \qquad \phi_n\big|_{x=0,L} = 0, \quad \textbf{(T)}$$

where $\Upsilon(\mathscr{P}) = 1 - \frac{\mathscr{P}}{p*}$, $\mathscr{P}(\phi_n) = \frac{\nu}{\nu-1}\left(\frac{\phi_n}{\phi_*}\right)^{\nu-1}$ and $\mathscr{Q}'(\phi_n) = \frac{\nu^2}{\nu-1}\left(\frac{\phi_n}{\phi_*}\right)^{\nu-1}$. We recover the equation investigated in [45]. In particular, analyzing the regime where ν tends to ∞ makes a connection appear with models based on free boundary problems. We also refer to [23] for an extension of this

analysis when nutrient are taken into account.

Figure 3 shows the evolution of the tumor volume fraction driven by (**T**), set on the computational domain $[-1.5, 1.5]$. We discuss the role of the exponent ν for the packing (homeostatic) pressure, by comparing the profile of the solutions obtained with $\nu = 5$ (panel (a)), $\nu = 20$ (panel (b)) and $\nu = 50$ (panel (c)) for the common threshold $\phi_* = .7$. We remind the reader that the biomechanical mechanisms acting on the tumor growth are embodied in these two parameters: they describe how the increase of the tumor volume fraction acts on the motion and the proliferation of the tumor cells. A further strain-stress analysis in the TME can be found in [44]. On Fig. 3-(a), the value $\nu = 5$ reflects a low stress on the tumor; we observe a growth of the volume fraction of the tumor ϕ_n with a smooth front which extends progressively as time increases, reaching saturation on the whole domain $[-1.5, 1.5]$ at $t = 6$. Fig. 3-(b), ν is moderately large ($\nu = 20$), and the stress exerted on the tumor becomes higher. The volume fraction of the tumor grows and reaches the saturation threshold at the centre of the domain quite rapidly compared to the previous case ($\nu = 5$): at $t = 4$, a saturated plateau has appeared. This saturation forms a steep front that propagates into the computational domain. Fig. 3-(c), ν is large ($\nu = 50$), and high tumor cells concentrations appear more rapidly: at $t = 2$ the tumor volume fraction ϕ_n is already close to the threshold ϕ_* with a steep front. This steep front reaches saturation at $t = 4$. However, the front propagates less rapidly into the computational domain compared to the case $\nu = 20$. Hence, the choice of a higher ν leads to higher tumor cell concentrations with sharp fronts. These observations are in line with the conclusions of [45].

3.2. Tumor cells subjected to the antitumor immune response in a passive environment (model (**T.A.**)*)*

We add to the previous model the action of the antitumor immune cells. Protumoral immune activities are neglected ($\phi_p = 0$) and we still assume $\phi_n, \phi_a \ll \phi_m \simeq 1$, so that the environment is supposed to be in a constant homogeneous state. Similarly, the nutrient supply is considered as given.

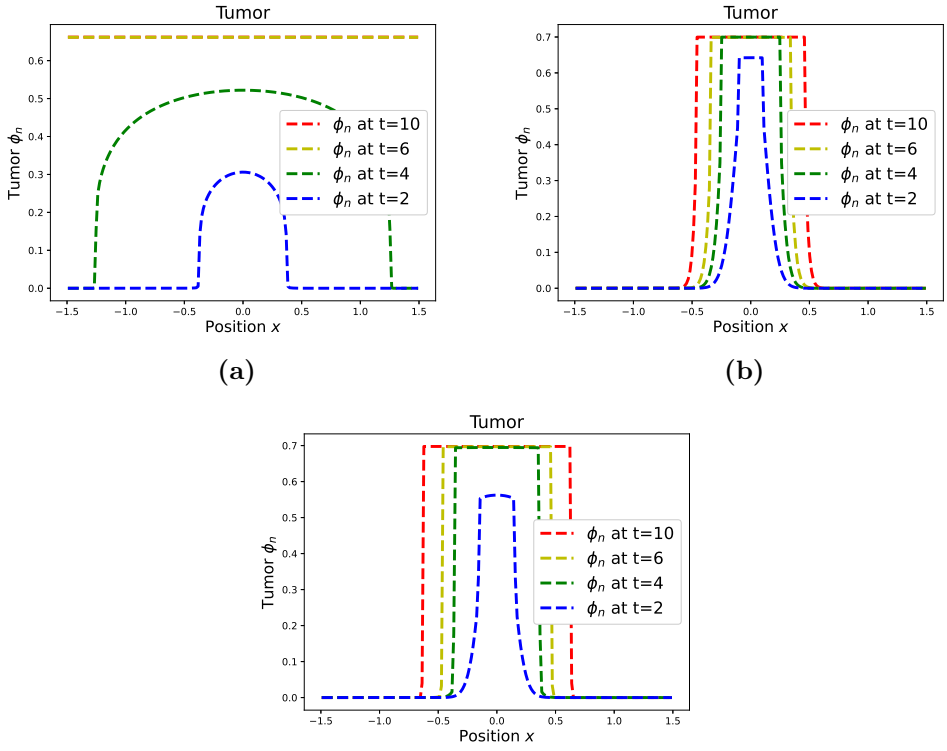

Figure 3: Simulation of the scalar equation (**T**): evolution of the tumor volume fraction ϕ_n on a domain $[-1.5, 1.5]$. Profiles at times $t = 2$, 4, 6, 10, with several exponents for the pressure law $\nu = 5$ (a), $\nu = 20$ (b) and $\nu = 50$ (c). Choosing large ν's leads to tumors with a saturated volume fraction and the formation of a neat propagating front

Therefore, the dynamic is governed by the following coupled system for ϕ_n, ϕ_a

$$\begin{aligned}
&\partial_t(\rho_n\phi_n) - \partial_x\left(\frac{\rho_n}{\lambda_{nm}}\mathscr{Q}'(\phi_n)\partial_x\phi_n\right) = \frac{\rho_n\phi_n}{\tau_n}(\Upsilon(\mathscr{P}) - A_a\phi_a),\\
&\partial_t(\rho_a\phi_a) + \partial_x\left(\frac{\chi_a}{\lambda_{am}}\rho_a\phi_a\partial_x\Phi - \frac{\rho_a D_a}{\lambda_{am}}\partial_x\phi_a\right) = \rho_a g\left(\int \rho_n\phi_n \,\mathrm{d}x\right) S_a - \gamma_a\rho_a\phi_a,\\
&\phi_n\big|_{x=0,L} = 0, \qquad \phi_a\big|_{x=0,L} = 0.
\end{aligned}$$

(T.A.)

We remind the reader that $\mathscr{P} = \frac{\nu p_*}{\nu-1}\Big(\frac{\phi_n}{\phi_*}\Big)^{\nu-1}$, $\Upsilon(\mathscr{P}) = 1 - \frac{\mathscr{P}}{p_*}$ and $\mathscr{Q}'(z) = z\mathscr{P}'(z) + \mathscr{P}(z)$. The chemotaxis potential is defined by

$$-\partial_x(D_\Phi \partial_x \Phi) = \rho_n\Big(\phi_n - \frac{1}{|\Omega|}\int \phi_n \,\mathrm{d}x\Big), \qquad \partial_x\Phi\big|_{x=0,L} = 0.$$

Here, we consider only space homogeneous sources of immune cells (being aware that space organization can be influential in shaping the immune response [5]), while we will discuss the role of space inhomogeneities for nutrient/oxygen. The evolution of the volume fractions of the tumor ϕ_n and of the antitumor immune cells ϕ_a is plotted in Figure 4. The antitumor response rapidly reduces the tumor volume fraction, which then forms two symmetric peaks. These peaks are pushed towards the edges of the domain, which, in turn, attract immune cells. Eventually, with some slight oscillations (see Figure 4), plateaus appear, with a non zero tumor volume fraction kept under control by the immune cells. This indicates the ability of the model in reproducing elimination/equilibrium phases. Here, the formation of peaks and their displacement towards the boundaries is not limited since the interaction with the environment is poorly described in the reduced model (**T.A.**).

3.3. Tumor-environment coupling and role of nutrient supply (model (**T.E.O.**)*)*

We go back to the situation where the immune response is disregarded ($\phi_a = \phi_p = 0$), but now we take into account the coupling with the environment. On the one hand, we work with the two volume fractions ϕ_n and $\phi_m = 1 - \phi_n$, and the velocity-pressure pair (V_m, Π). On the other hand, we take into account the oxygen/nutrient supply. Namely, we are dealing with

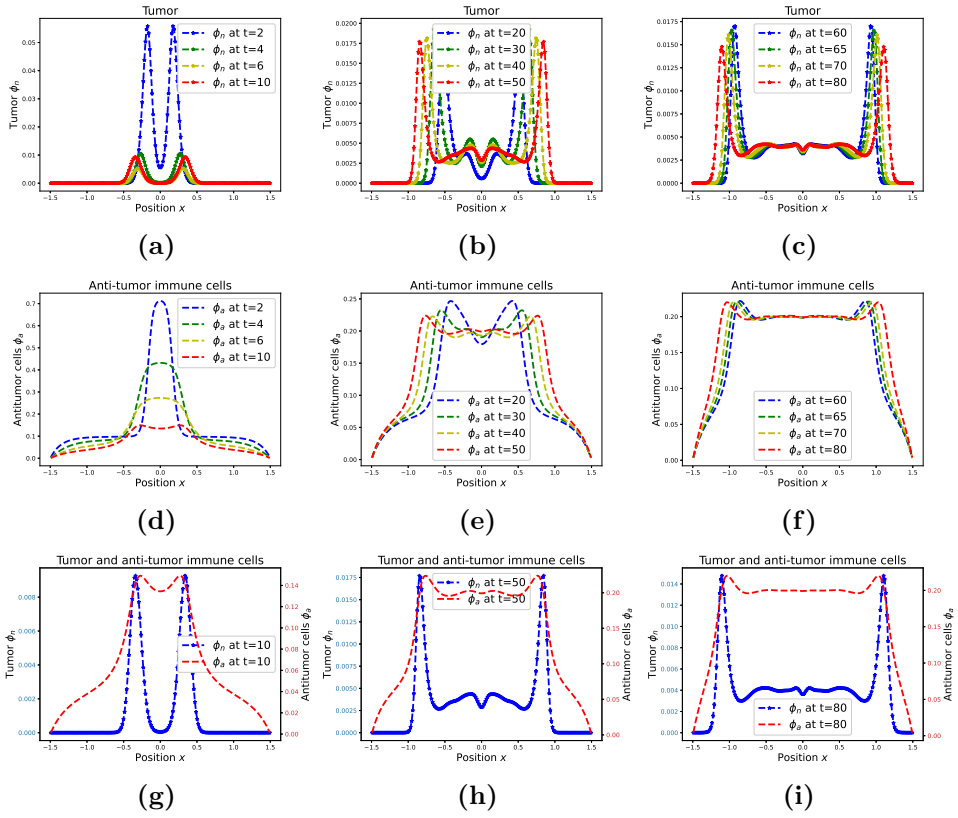

Figure 4: Simulations of the coupled tumor-antitumor immune cells system model (**T.A.**). Evolution of the tumor volume fraction ϕ_n (a-c) and the antitumor immune cells volume fraction ϕ_a (d-f), represented at several times: $t = 2,\ 4,\ 6,\ 10$ (a,d), $t = 20,\ 30,\ 40,\ 50$ (b,e), $t = 60,\ 65,\ 70,\ 80$ (c,f) with $\nu = 50$. Space repartition at time $t = 10$ (g), $t = 50$ (h) and $t = 80$ (i) of the tumor and immune cells. The tumor cells are eliminated and pushed away by the action of the immune cells (mind that scale are different as time evolves)

the following system:

$$
\begin{aligned}
&\partial_t(\rho_n\phi_n) + \partial_x\Big(\rho_n\phi_n\Big(V_m - \frac{\partial_x\Pi}{\lambda_{nm}(1-\phi_n)}\Big)\Big) - \partial_x\Big(\frac{\rho_n\mathscr{Q}'(\phi_n)}{\lambda_{nm}(1-\phi_n)}\partial_x\phi_n\Big) \\
&\qquad\qquad = \frac{\rho_n\phi_n}{\tau_n}\Upsilon(\mathscr{P}, O), \\
&-\frac{\varpi_m}{\rho_m}\partial^2_{xx}V_m + \partial_x\Pi + \partial_x(\phi_n\mathscr{P}) = 0, \\
&\partial_x\left(V_m - \frac{\phi_n\partial_x\Pi + \partial_x(\phi_n\mathscr{P})}{\lambda_{nm}(1-\phi_n)}\right) = \frac{\phi_n}{\tau_n}[\Upsilon]_+ - \Big(1 - \frac{\rho_n}{\rho_m}\Big)\frac{\phi_n}{\tau_n}[\Upsilon]_-, \\
&-\partial_x(D_O\partial_x O) + \partial_x\left(O\chi_O\partial_x\phi_n\right) = S_O - O(r_n\rho_n\phi_n + r_m\rho_m(1-\phi_n)),
\end{aligned}
$$

$$
\begin{aligned}
&\phi_n\big|_{x=0,L} = 0, \quad V_m\cdot\nu_x\big|_{x=0,L} = \int_0^L\Big(\frac{\Gamma_a}{\rho_a} + \frac{\Gamma_p}{\rho_p} + \frac{\Gamma_n}{\rho_n} + \frac{\Gamma_m}{\rho_m}\Big)\,\mathrm{d}x, \\
&O\big|_{x=0,L} = O_{bd}.
\end{aligned}
$$

(T.E.O.)

The functions $\mathscr{P}$ and $\mathscr{Q}$ are defined as before, and, in the right hand side,

$$\Upsilon(\mathscr{P}, O) = k_{+O}[O - O^*]_+ - \Big(k_{-O}[O - O_*]_- + \frac{\mathscr{P}}{p_*}\Big).$$

In order to assess the influence of the source of the oxygen-nutrient supply, we perform simulations with the source S_O given by one of the following formula:

$$\text{homogeneous source: } S_O(x) = \frac{1}{3}, \tag{20a}$$

inhomogeneous source centered at the hotbed of the tumor:

$$S_O(x) = \frac{1}{\sigma\sqrt{2\pi}} \exp\left(-\frac{x^2}{2\sigma^2}\right), \tag{20b}$$

inhomogeneous source centered far from the hotbed of the tumor:

$$S_O(x) = \frac{\mathcal{R}(x)}{\displaystyle\int_0^L \mathcal{R}(x)\mathrm{d}x}, \tag{20c}$$

$$\mathcal{R}(x) = \sum_{j=1}^{2} \frac{k_j}{\sigma_j\sqrt{2\pi}} \exp\left(-\frac{1}{2}\left(\frac{x - m_j}{\sigma_j}\right)^2\right),$$

with k_1, k_2, σ, σ_1, σ_2 positive numbers and m_1, m_2 given locations in the computational domain. For the simulations, we set $\sigma_1 = \sigma_2 = 0.4$, $k_1 = k_2 = 1$, $m_1 = -1$, and $m_2 = +1$. Note that these data are normalized so that they provide the same total amount of nutrient. Therefore, we are going to discuss the influence of

- the thresholds O_* (necrotic threshold) and O^* (proliferation threshold), together with the role of the stress exerted on the tumor described by the parameter ν;
- the ability of the tumor in attracting oxygen-nutrient supplies, embodied into the strength of the parameter χ_O, and the role of the parameter f_* describing the degradation of the environment by cytokines;
- the location of the oxygen-nutrient sources compared to the initial location of the tumor,

In Figure 5, we compare two types of environment which are not very favorable to the tumor development: we set $O^* = .8$ (proliferation threshold), $\chi_O = .5$ (chemotactic coefficient) and the delocalized source (20c); we represent both the tumor volume fraction (a, b, e, f, i, j) and the nutrients concentration (c, d, g, h, k, l). Figures (a, c, e, g, i , k) correspond to a *moderately oxygenated environment*, with necrotic threshold $O_* = 0$, while figures (b, d, f, h, j, l) correspond to a *hypoxic environment* with a positive necrotic threshold $O_* = .6$. In order to make the effects more visible, we have multiplied for this simulation the initial volume fraction of tumor cells (19) by a factor of 5: this leads to a higher tumor volume fraction. Moreover, we make the exponent ν increase. On figures (a,b,c,d), $\nu = 5$ corresponds to a low stress on the tumor. The tumor volume fraction decreases due to the combined effects of the homeostatic pressure, the diffusion and the lack of oxygen and nutrients to sustain its development: the concentration O remains below the proliferation threshold O^*. In the hypoxic environment, this effect is even more sensitive since the concentration O is also below the necrotic threshold O_*, despite the sensitive attraction exerted by the tumor. This has to be compared to Figure 3-(a) where a constant supply boosts the tumor development. Increasing ν ($\nu = 7$ for figures (e, f, g, h)) damps these effects. When ν is large ($\nu = 50$ for figures (i, j, k, l)), the tumor volume fraction becomes stationary. This is due to the fact that the homeostatic terms $\mathscr{P}$ takes very small values when ϕ_n is below the threshold ϕ_*, so that the death term in the equation for ϕ_n almost vanishes. Note that it might occur, in the hypoxic environment, see Figure (l), that the tumor volume fraction becomes high enough to attract oxygen and nutrients above the necrotic threshold at the center of the domain.

These effects are confirmed in Figure 6 which represents the evolution of the total mass in these configurations (a, b), and for the initial volume fraction of tumor cells (19) (c, d). In the latter case, the tumor volume fraction is too low to attract oxygen and the tumor remains in a hypoxic environment.

Next, we discuss how certain mechanisms can help the tumor in developing despite the environment is not favorable to its expansion, either by attracting oxygen and nutrient (effect of the chemotactic coefficient χ_O) or through the degradation of the environment by proteases/cytokines (effect of the parameter f_*).

In Figure 7, we set $O^* = .8$ (proliferation threshold), $O_* = .6$ (necrotic

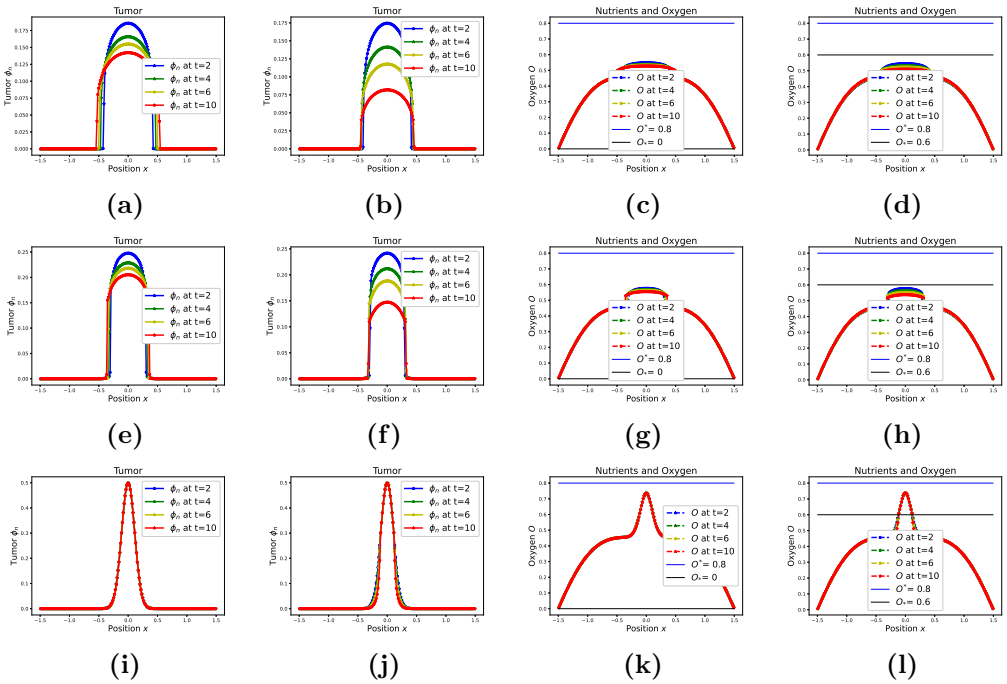

Figure 5: Simulation of the coupled model (**T.E.O.**): profile of the tumor volume fraction ϕ_n and the oxygen concentration O. Proliferation threshold $O^* = .8$, $\chi_O = .5$ and S_O given by (20c), (a-c-e-g-i-k): the case where necrotic threshold $O_* = 0$, (b-d-f-h-j-l): the case where necrotic threshold $O_* = .6$. The initial data (19) is multiplied by 5. Figures (a-b-c-d) correspond to the case $\nu = 5$, (e-f-g-h) to $\nu = 7$ and (i-j-k-l) to $\nu = 50$

threshold), $f_* = 0$ and S_O is given by (20c). On figures (a, c, e), we have $\chi_O = .5$ and the tumor extincts due to a lack of supplies, the concentration O being below the necrotic threshold on the whole domain. On figures (b, d, f), we have $\chi_O = 3.4$ which allows the tumor to attract oxygen-nutrient towards the center of the domain; the oxygen concentration passes above the proliferation threshold O^* so that the tumor can grow (at $t = 2$), eventually reaching saturation, and it expands, with the formation of a steep front (at $t = 10$). The observations are confirmed by the velocity profiles on the Figure 7-(e, f): the velocity field V_n vanishes in the situation of low attractiveness while it reveals the tumor expansion towards the edges of the domain when χ_O is larger. This example shows that the ability of the tumor in developing access to nutrient and oxygen is a key feature of tumor growth reproduced by the model.

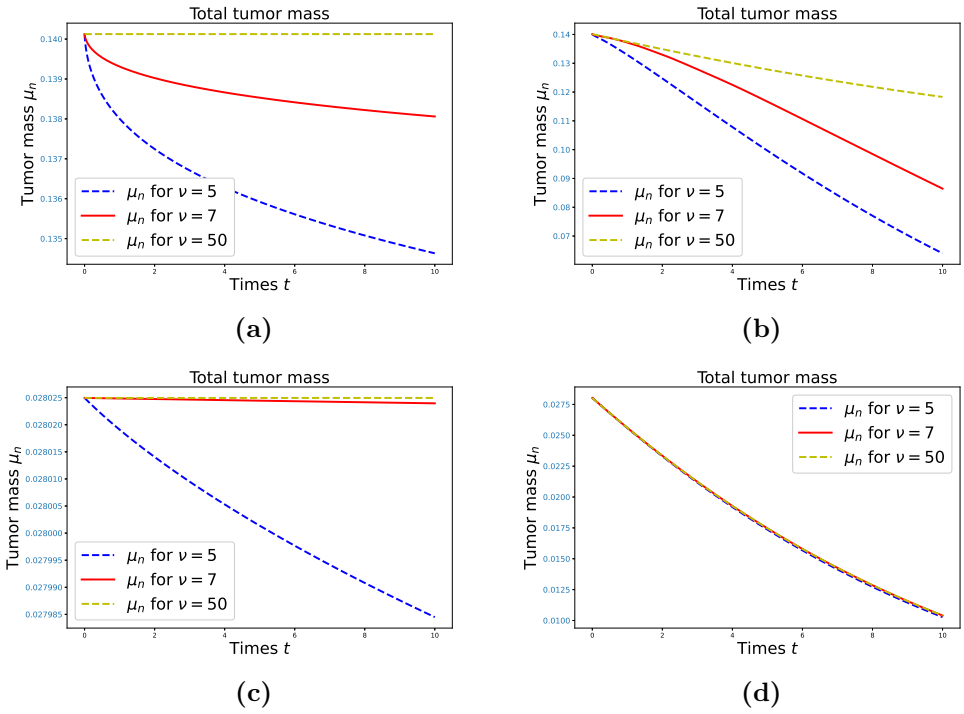

Figure 6: Simulation of the coupled model (**T.E.O.**), evolution of the total tumor mass ϕ_n for several values of ν. Proliferation threshold $O^* = .8$, $\chi_O = .5$ and S_O given by (20c); (a-c): necrotic threshold $O_* = 0$, (b-d): necrotic threshold $O_* = .6$; (a-b): initial data $5\times(19)$, (c-d): initial data (19)

Figure 8 illustrates that the degradation of the environment equally fosters the development of the tumor, despite an environment lacking of oxygen and nutrient supply. The parameters are the same as in Figure 7, with $\chi_O = .5$ on (a, c, e), and $\chi_O = 3.4$ on (b, d, f), but now we have set $f_* = .1$. In Figure 8-(a, c, e) we see that the degradation of the environment by proteases/cytokines leaves room for the tumor and the oxygen concentration slightly overtakes the proliferation threshold in the center of the domain. This effect is limited and the tumor stabilizes (from $t = 4$) because its attractiveness χ_O is not high enough. The representation of the total mass of the tumor in Figure 8-(e) shows that the tumor remains under control. Figure 8-(b, d) has to be compared to Figure 7-(b, d): the saturation of the tumor volume fraction holds more rapidly as it can be also seen on the

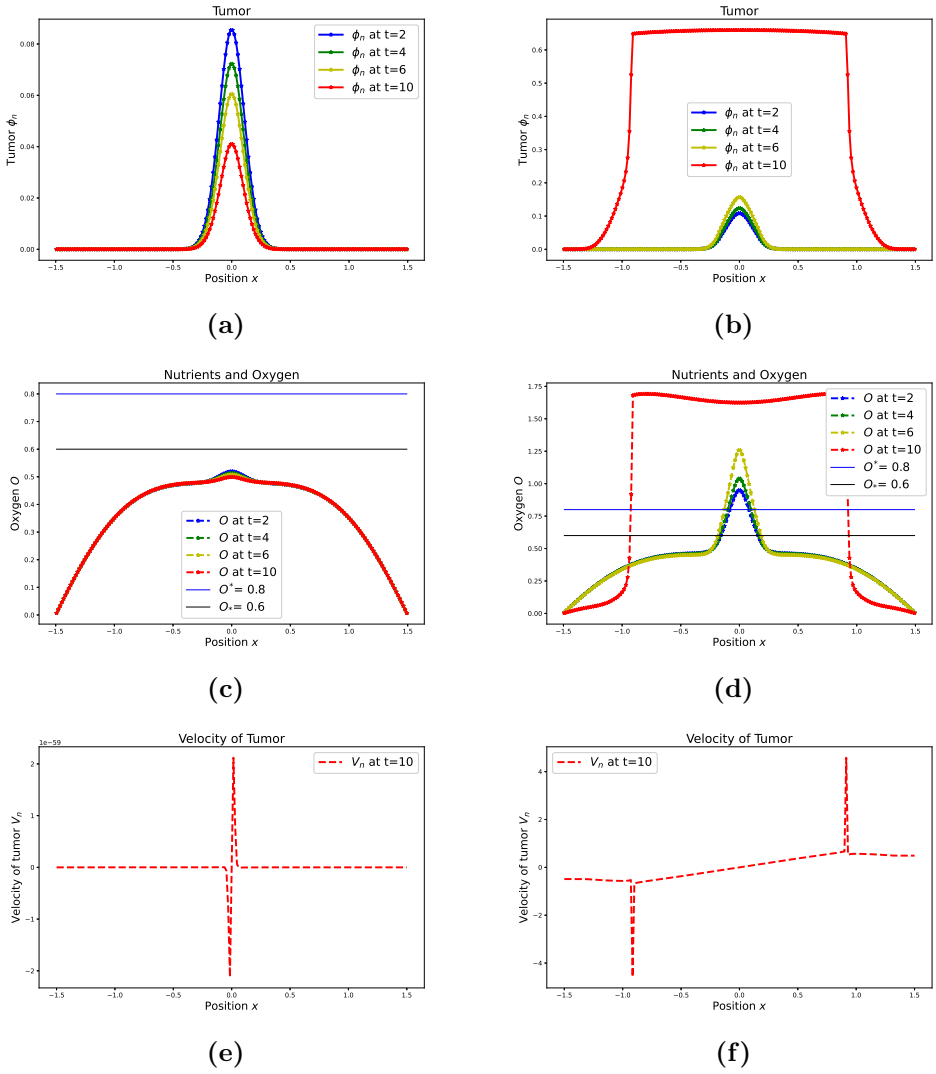

Figure 7: Simulation of the coupled model (**T.E.O.**): profile of the tumor volume fraction ϕ_n, the oxygen concentration O and velocity of tumor cells V_n. Proliferation threshold $O^* = .8$, necrotic threshold $O_* = .6$, $f_* = 0$ and S_O given by (20c); (a-c-e): $\chi_O = .5$ (controlled tumor), (b-d-f): $\chi_O = 3.4$ (uncontrolled tumor); with a stress on tumor $\nu = 50$.

evolution of the total tumor mass in (f).

Finally, in Figure 9, we consider different types of sources: (20c) in (a, d, g, j), (20b) in (b, e, h, k) or (20a) in (c, f, i, l). We compare the case where

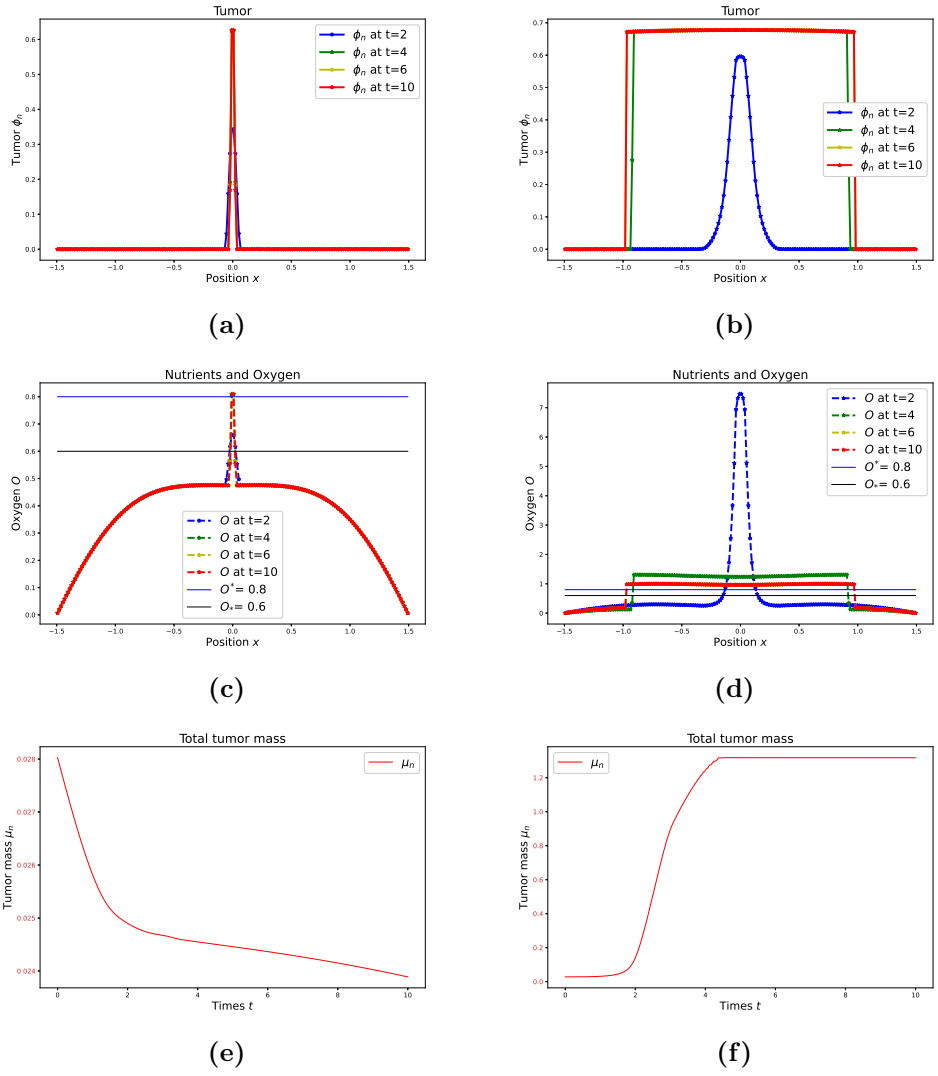

Figure 8: Simulation of the coupled model (**T.E.O.**): profile of the tumor volume fraction ϕ_n, the oxygen concentration O and time evolution of total tumor mass μ_n for different values of χ_O. Proliferation threshold $O^* = .8$, necrotic threshold $O_* = .6$, $f_* = .1$ and S_O given by (20c); (a-c-e): $\chi_O = .5$ (controlled tumor), (b-d-f): $\chi_O = 3.4$ (uncontrolled tumor); with a stress on tumor $\nu = 50$

we neglect the effect of proteases/cytokines on the environment ($f_* = 0$) and the case where we consider environment degradation ($f_* = .1$). We can see that a source of nutrient close to the tumor provides much more favorable conditions for the tumor to grow than sources situated a little far away, for a given attraction capacity ($\chi_O = .5$ on (a-f), or $\chi_O = 3.4$ on (g-l)). We also confirm the influence of the degradation of the environment: this is sensitive for instance when comparing a homogeneous source, where taking into account the degrading action of proteases/cytokines produces a dramatic increase of the tumor mass, see Figure 9-(c). The worst situation is illustrated in Figure 9-(j, k, l): the high chemotactic coefficient χ_O, combined to the action of the cytokines, always leads to a growth of the tumor mass, no matter where the source is located.

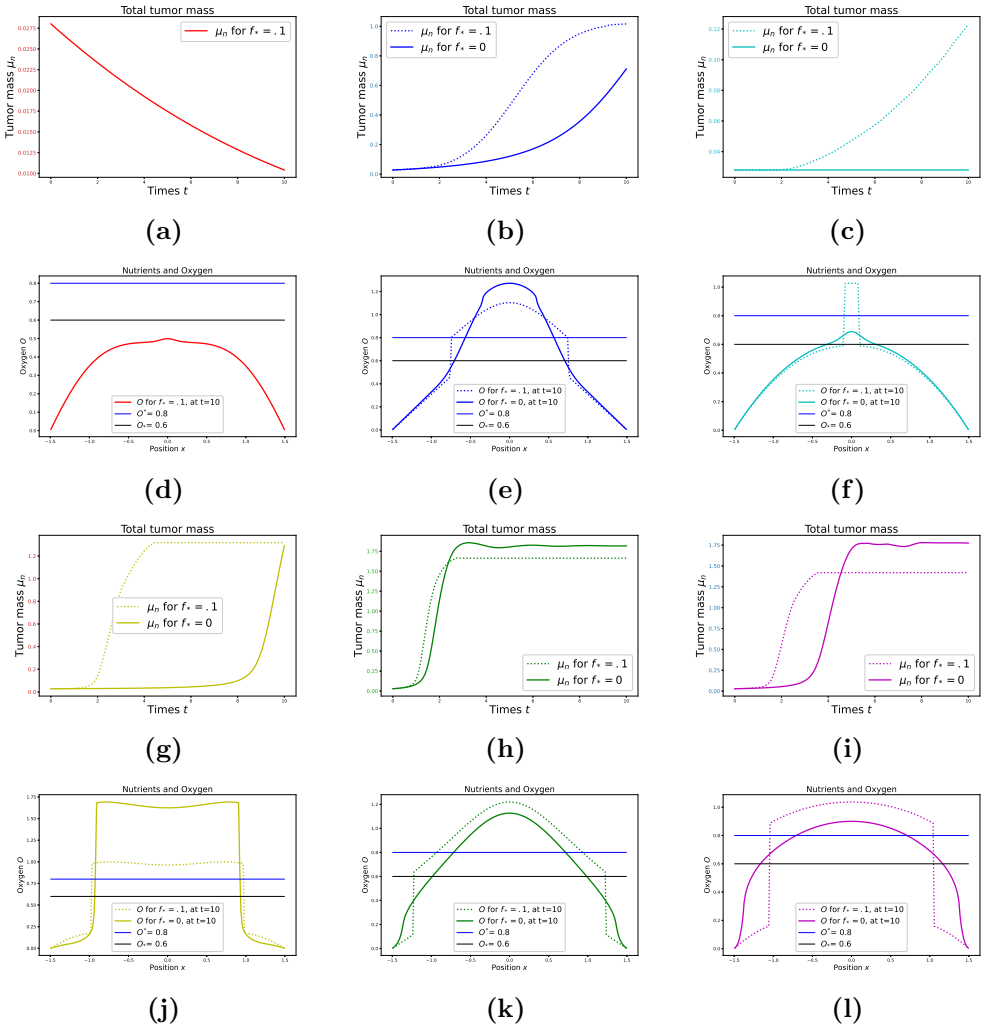

Figure 9: Simulation of the coupled model (**T.E.O.**): time evolution of total tumor mass μ_n and profile of oxygen concentration at time $t = 10$ for different choices of χ_O and S_O. Proliferation threshold $O^* = .8$, necrotic threshold $O_* = .6$. (a-d-g-j): inhomogeneous delocalized source (20c), (b-e-h-k): inhomogeneous source located next to the original tumor (20b), (c-f-i-l): homogeneous source (20a); (a) to (f): $\chi_O = .5$, (g) to (l): $\chi_O = 3.4$; with a stress on tumor $\nu = 50$

3.4. Antitumor immune response in a complex environment: equilibrium phases (model (**T.A.E.O.**)*)*

We now take into account the antitumor action of the immune system: this corresponds to our goal to simulate the dynamics of "hot" tumors, char-

acterized by an infiltration of the TME by immune cells. Therefore, the model reads

$$
\begin{aligned}
&\partial_t(\rho_n\phi_n) + \partial_x\Big(\rho_n\phi_n\Big(V_m - \frac{\partial_x\Pi}{\lambda_{nm}\phi_m}\Big)\Big) - \partial_x\Big(\frac{\rho_n\mathscr{D}'(\phi_n)}{\lambda_{nm}\phi_m}\partial_x\phi_n\Big)\\
&\qquad\qquad = \frac{\rho_n\phi_n}{\tau_n}(\Upsilon(\mathscr{P},O) - A_a\phi_a),\\
&\partial_t(\rho_a\phi_a) + \partial_x\Big(\rho_a\phi_a\Big(V_m - \frac{\partial_x\Pi}{\lambda_{am}\phi_m} + \frac{\chi_a}{\lambda_{am}\phi_m}\partial_x\Phi\Big)\Big) - \partial_x\Big(\frac{\rho_a D_a}{\lambda_{am}\phi_m}\partial_x\phi_a\Big)\\
&\qquad\qquad = \rho_a g\left(\int \rho_n\phi_n \,\mathrm{d}x\right) S_a - \rho_a\phi_a\gamma_a.\\
&-\partial_x(D_O\partial_x O) + \partial_x\left(O\chi_O\partial_x\phi_n\right) = S_O - O(r_n\rho_n\phi_n + r_a\rho_a\phi_a + r_m\rho_m\phi_m)\\
&-\partial_x(D_\Phi\partial_x\Phi) = \rho_n\Big(\phi_n - \frac{1}{|\Omega|}\int \phi_n \,\mathrm{d}x\Big),\\
&-\frac{\varpi_m}{\rho_m}\partial_{xx}^2 V_m + \partial_x\Pi = -\partial_x(\phi_n\mathscr{P}) + (\phi_a\chi_a\partial_x\Phi - D_a\partial_x\phi_a),\\
&\partial_x\left(V_m - \Big(\frac{\phi_n}{\phi_m\lambda_{nm}} + \frac{\phi_a}{\phi_m\lambda_{am}}\Big)\partial_x\Pi - \frac{1}{\phi_m\lambda_{nm}}\partial_x(\phi_n\mathscr{P})\right.\\
&\qquad\qquad \left. + \Big(\frac{\phi_a\chi_a}{\phi_m\lambda_{am}}\Big)\partial_x\Phi - \frac{D_a}{\phi_m\lambda_{am}}\partial_x\phi_a\right)\\
&\qquad\qquad = \frac{\Gamma_a}{\rho_a} + \frac{\Gamma_n}{\rho_n} + \frac{\Gamma_m}{\rho_m},\\
&\phi_n\big|_{x=0,L} = 0, \qquad \phi_a\big|_{x=0,L} = 0,\\
&V_m\cdot\nu_x\big|_{x=0,L} = \int_0^L \Big(\frac{\Gamma_a}{\rho_a} + \frac{\Gamma_p}{\rho_p} + \frac{\Gamma_n}{\rho_n} + \frac{\Gamma_m}{\rho_m}\Big)\,\mathrm{d}x,\\
&\partial_x\Phi\big|_{x=0,L} = 0, \qquad O\big|_{x=0,L} = O_{bd}.
\end{aligned}
$$

(**T.A.E.O.**)

Note that oxygen/nutrient consumption arises from tumor cells and antitumor immune cells as well as the environment. Hence there is both a competition for space and a competition for resources. We consider an environment where oxygen and nutrient are available, in order to assess whether or not the antitumor response is able to control the tumor growth in such a favorable situation. For the simulation, we have chosen a substantially higher uptake from the tumor cells, since they are known to be highly glycolytic [36], due to their proliferation activity.

We are also going to discuss the effect of the degradation of the environment, which can be an important ingredient in the quest for space.

We start by assuming $f_* = 0$ (no degradation). Results are displayed in

Figure 10, with $\chi_O = .5$ (low chemotactic coefficient, (a, c, e)) and $\chi_O = 3.4$ (high chemotactic coefficient, (b, d, f)). The tumor is rapidly eliminated, especially for delocalized (20c) and homogeneous (20a) sources. This is coherent with Figure 9-(a, b, c): in such conditions, the growth of the tumor is already difficult without immune response. With a high chemotactic coefficient, we observe an important elimination of the tumor cells in the center of the domain, when the source itself is centered, see Figure 10-(b, d, f). This is because the strength of the antitumor immune cells on the tumor is quite high ($A_a = 5$) and the intensity of the antitumor source is also high ($S_a = 3$). This situation, where the tumor is thus controlled has to be compared to Figure 9-(j, k, l) where, in absence of antitumor action, the tumor was able to escape.

In Figure 11, we add the action of proteases/cytokines on the environment ($f_* = .1$). In the tested configuration, it does not modify substantially the evolution of the total tumor mass, which is eventually eliminated (whatever the value of χ_O), showing the strength of the antitumor immune response is a dominant parameter. The profile for the oxygen/nutrient concentration does not significantly differ from Figure 10. The main effect however is to impact the space repartition of the tumor, which is more localized, with more peaked values of the volume fraction when the proteases/cytokines are activated. The degradation of the environment produces sharper profiles of the tumor concentration.

It is also worth investigating the large time behavior of the system, to study whether the tumor is completely eliminated or remains in a residual equilibrium state. This is the object of Figure 12 and 13, the latter taking into account the possible degradation of the environment by proteases/cytokines. In cases where the source of oxygen is localized in the vicinity of the tumor, such an equilibrium forms. But for delocalized and homogeneous sources, the nutrient supply is too low to sustain the presence of tumor cells and all populations (tumor and immune cells) eventually disappear.

3.5. Simulation of the full model: from equilibrium to escape

Eventually, we perform simulation of the full model defined in Section 2.5, with both anti- and protumor immune responses. As in [5], we see that the intensity of the source of the antitumor immune cells is critical to determine whether the tumor is controlled or escape.

We compare in Figure 14 the behavior obtained for several values of a (homogeneous) source of antitumor immune cells $S_a = 3$, $S_a = 3/10$(a, c,

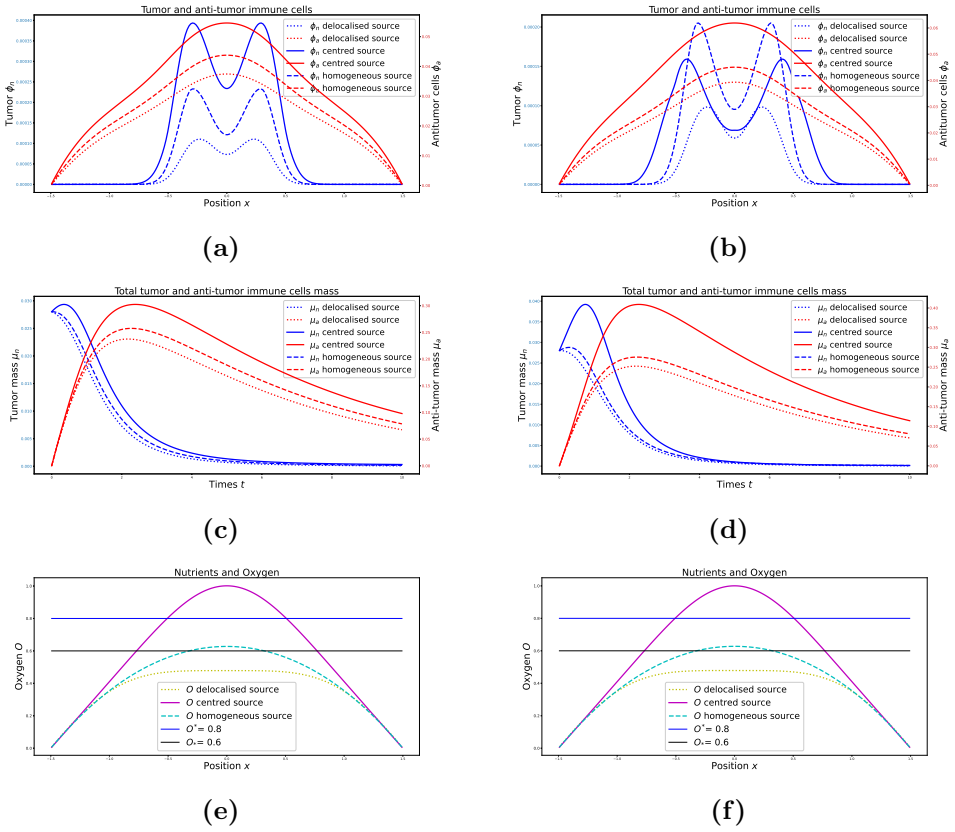

Figure 10: Simulation of the coupled model (**T.A.E.O.**): profile of the tumor and antitumor cells volume fraction ϕ_n and ϕ_a, the oxygen concentration O and time evolution of the total mass of the tumor μ_n and antitumor cells μ_a for different choices of χ_O and S_O. Proliferation threshold $O^* = .8$, necrotic threshold $O_* = .6$, $f_* = 0$. We make the chemotactic coefficient χ_O vary: (a-c-e) $\chi_O = .5$, (b-d-f): $\chi_O = 3.4$; with $\nu = 50$, $A_a = 5$, $r_n = .9$, $r_m = r_a = r_n/10$. Evolution in short time ($t = 10$)

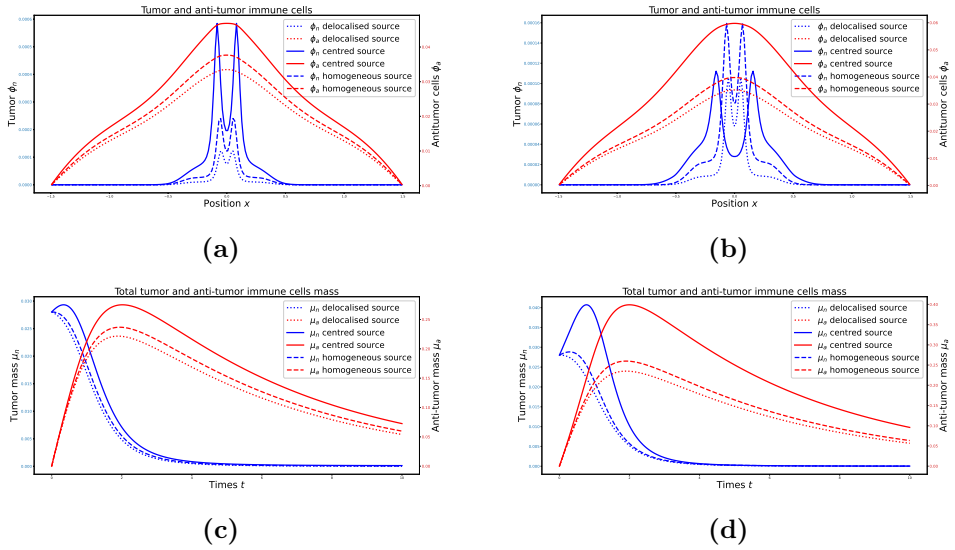

Figure 11: Simulation of the coupled model (**T.A.E.O.**): profile of the tumor and antitumor cells volume fraction ϕ_n and ϕ_a and time evolution of the total mass of the tumor μ_n and antitumor cells μ_a for different choices of χ_O and S_O with positive $f_* = .1$. Proliferation threshold $O^* = .8$, necrotic threshold $O_* = .6$. We make the chemotactic coefficient χ_O vary : (a-c): $\chi_O = .5$, (b-d) $\chi_O = 3.4$; with $\nu = 50$, $A_a = 5$, $r_n = .9$, $r_m = r_a = r_n/10$. Evolution in short time ($t = 10$)

e, g) and $S_a = 3$, $S_a = 3/1000$ (b, d, f, h), all the other parameters being unchanged. With $S_a = 3$, the tumor is controlled by the antitumor immune response, despite the presence of protumor immune cells which are not sufficient to help the tumor to grow. When $S_a = 3/10$, see Figure 14-(a, c, e, g), we observe a higher volume fraction of protumor immune cells, and thus a higher tumor volume fraction too, in the transient states. When $S_a = 3/1000$, see Figure 14-(b, d, f, h) (mind the change of scale for the tumor volume fraction), we observe that the tumor escapes: its volume fraction reaches saturation and forms a steep front. Note that both anti- and protumor immune cells remain concentrated at the center of the domain.

3.6. How changes of key parameters select tumor-immune system scenario

Having set up through numerical experiments the role of the parameters of the model, we now wish to provide a more in-depth discussion on the selection between different scenarios. To this end, we limit the discussion

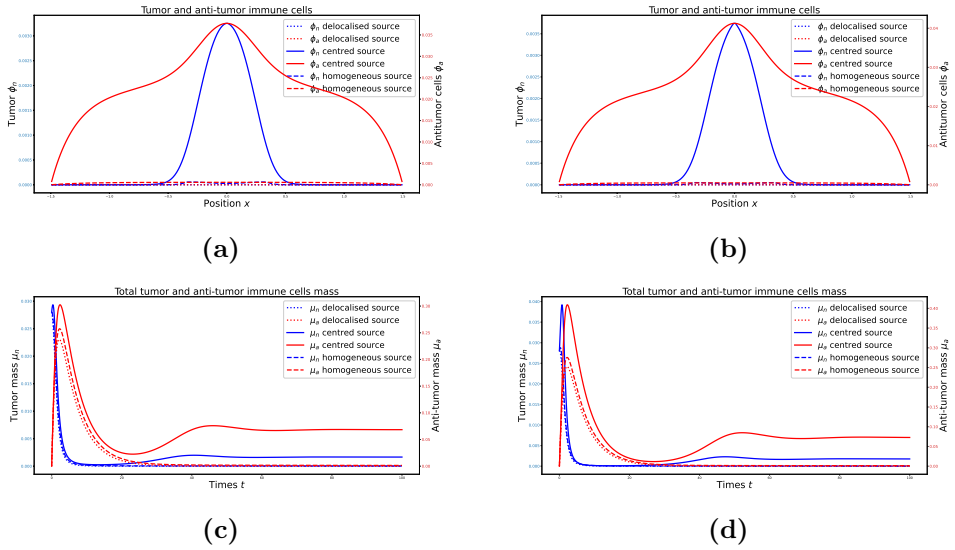

Figure 12: Simulation of the coupled model (**T.A.E.O.**): profile of the tumor and antitumor cells volume fraction ϕ_n and ϕ_a and time evolution of the total mass of the tumor μ_n and antitumor cells μ_a for different choices of χ_O and S_O. Proliferation threshold $O^* = .8$, necrotic threshold $O_* = .6$, $f_* = 0$. We make the chemotactic coefficient χ_O vary: (a-c) $\chi_O = .5$, (b-d): $\chi_O = 3.4$; with $\nu = 50$, $A_a = 5$, $r_n = .9$, $r_m = r_a = r_n/10$. Evolution in long time ($t = 100$)

to the modulation of two parameters only: the chemotactic coefficient χ_O, that is the ability of tumor cells to attract nutrients, and the amplitude of the source S_a of antitumor immune cells, This choice is motivated by our preliminary investigations that confirm the intuition that these parameters are likely the most influential in driving efficient control of tumor growth. It is also consistent with clinical observations; indeed, the mode of action of certain treatments can be translated as a modification of these parameters. For instance, increasing the concentration of some interleukins (like IL-2) is a strategy used to strengthen the immune response by stimulating the proliferation of effector cells, a strategy efficient but with a scope limited by a significant toxicity. Therapeutic vaccination or administration of immune checkpoint inhibitors are other ways to stimulate the antitumor immune response. These actions are reflected in the equations by a strengthening of the terms of activation and recruitment of effector immune cells. Similarly, the reduction of the nutrients attraction capability of tumor cells can also

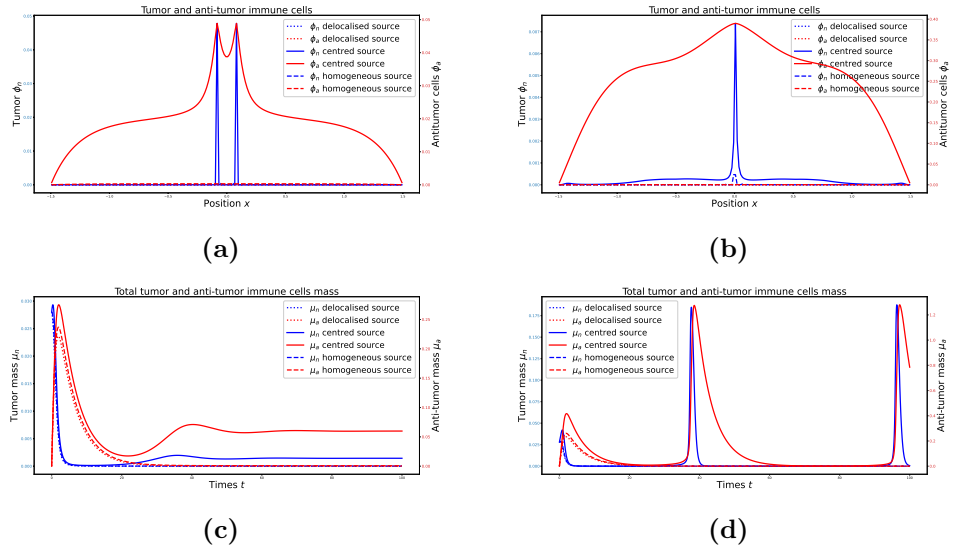

Figure 13: Simulation of the coupled model (**T.A.E.O.**): profile of the tumor and antitumor cells volume fraction ϕ_n and ϕ_a and time evolution of the total mass of the tumor μ_n and antitumor cells μ_a for different choices of χ_O and S_O with positive $f_* = .1$. Proliferation threshold $O^* = .8$, necrotic threshold $O_* = .6$. We make the chemotactic coefficient χ_O vary: (a-c): $\chi_O = .5$, (b-d): $\chi_O = 3.4$; with $\nu = 50$, $A_a = 5$, $r_n = .9$, $r_m = r_a = r_n/10$. Evolution in long time ($t = 100$)

be the result of treatments, like anti-VEGF that reduce angiogenesis at the expense of tumor growth.

To discuss parameters influence, we construct "heat maps" in the (χ_O, S_a)-plane according to the mean value of the total tumor mass μ_n, see (6), on a given observation time T, chosen sufficiently large

$$\frac{1}{T}\int_0^T \mu_n(t)\,\mathrm{d}t.$$

This criterion allows us to discriminate between scenario where the tumor growth is damped by the immune response, or where the tumor proliferates. Nevertheless, while the obtained representations are quite suggestive, a finer analysis of the time evolution of the tumor mass reveals that oscillations can occur, with possibly quite high peaks between relapse episodes (see Figures 16 to 25). In order to evaluate the immune response, we similarly define $\mu_a = \int \rho_a \phi_a \,\mathrm{d}x$ and we will construct heat map of the antitumor reaction

from the mean value $\frac{1}{T}\int_0^T \mu_a(t)\,\mathrm{d}t$.

We start with the model (**T.A.E.O.**). Simulations are performed with S_O given by (20b) and $O^* = .8$, $O_* = .6$, $f_* = 0$, $\nu = 50$, $A_a = 5$, $r_n = .9$, $r_m = r_a = r_n/10$. Of course, the choice of the final time T is not harmless: Figures 15 are obtained for $T = 100$ (a) and $T = 200$ (b), and we do not see significant difference at this level. According to the intuition, low S_a and large χ_O are favorable to the tumor; increasing S_a or reducing χ_O reduce the mean tumor mass. Next, we make more details appear by zooming on different regions of the parameters. Spots on the heat maps indicate parameters for which the time evolution of the tumor mass and antitumor immune cells mass are displayed; the selection represents quite typical graphs in the considered domain. In Figure 16, we focus on $.001 \leq S_a \leq .1$ and $.5 \leq \chi_O \leq 2$. The extreme case, Figure 16-(b), can be considered as an escape phase, where the tumor has fully developed, since with these parameters the final situation is very close to the one obtained without immune response (model (**T.E.O.**), not represented: a stationary state is sharply reached with a final value $\mu_n \simeq 1.2$). In contrast, Figure 16-(d) corresponds to an equilibrium phase where the tumor mass is maintained at a low level. In Figure 17, we increase the range $.5 \leq \chi_O \leq 2$: for low values of S_a, of course, we still observe a fully developed tumor in Figure 17-(b). For higher values of S_a, like in Figure 17, the tumor is still controlled by the immune response, but there are oscillations of significant amplitude, slightly damped. In Figures 18 and 19 the range for S_a is quite high and we observe an equilibrium phase, possibly with small amplitude oscillations of the tumor mass.

Figure 20 shows the impact of the degradation of the environment with $f_* \neq 0$: escape holds faster and equilibrium can be perturbed, either reaching a higher final mass or by making peaked oscillations appear.

Next, we turn to the full model where protumor reactions are taken into account. We keep the parameters as above, except $f_* = 1$ in order to investigate the most favorable environment to the tumor and we have set $S_p = 3$ which means a significant activation of protumor immune cells. At first sight, the global landscape is similar to the one obtained with (**T.A.E.O.**): see Figure 21 at the final time $T = 100$ or $T = 200$; but we see a less effective effect of the increase of S_a, and a significantly higher presence of antitumor immune cells. In fact, the details of the time evolution of the tumor mass clearly reveal the dramatic effect of the protumor mechanisms, with marked oscillations, even in situations which were controlled with (**T.A.E.O.**), and

alternance of high peaks, the amplitude of which might increase, and relapse, with quite short periods: see Figures 22-25. These examples indicate that it is likely important to design treatments that target the protumor effects of the immune response, which can be obtained by blocking the MDSC (anti-CXCR2, cMet) and Tregs (anti-CD25) infiltration or by acting on cytokine signals.

4. Conclusion

We have set up a hydrodynamic model, inspired from mixture theory, describing the complex interactions in the TME, between tumor cells, immune cells, and the surrounding tissues. Beyond the elimination or enhanced proliferation mechanisms by the immune system, the equations describe the competition for space and the access to nutrient and oxygen. The model is challenged on numerical grounds, restricting to a simple one-dimensional geometry. The simulations bring out several key mechanisms, that are critical in shaping the tumor development and the efficacy of the immune response. The simplified framework discussed here already shows relevant effects related to the space organization of the TME, motivating a modeling based on PDEs. This preliminary attempt opens perspectives for a thorough discussion based on clinical data obtained by modern imagery techniques, that provide a quite precise description, at a given time, of the TME.

For the time being, the objectives of this work remain essentially qualitative rather than quantitative. An important issue is the calibration of the numerous parameters of the equations, which faces the fact that, while quite precise images of the TME are available, the temporal evolution is lacking. For this reason, we think that it is more important to extract the main drivers of the observed phenomena, with a reduced set of equations and parameters, than to incorporate further terms and species in the equations. Nevertheless, the study can shed some light on the key factors of the tumor growth and the immune response. It is indeed remarkable that the model reproduces behaviors coherent with the 3E's observations, while such trend have not been built-in a priori. Moreover, in the spirit of [5], it will be possible to identify on numerical grounds the role of treatments, how the doses, time of administration and combination impact the tumor development, for instance by reactivating hyporesponsive antitumor immune cells (by using Immune Checkpoint Inhibitors like anti-PD-1 or anti-CTLA4 antibodies) or

reducing the recruitment of protumor cells (by blocking Tregs infiltration with anti-CD25 or targeting MDSCs).

Appendix A. Numerical methods

The discretization of the equations is based on the Finite Volume framework, which is intended to mimic at the discrete level the balance relations over a fixed domain that lead to the derivation of the fluid mechanics equations. We are going to use *staggered discretizations* where the discrete unknowns can be stored at different locations, depending on their physical meaning. This allows us to handle appropriately the incompressibility constraint, in the spirit of the MAC scheme [33]. The scheme we present here is inspired from [20, 46] and it is implemented in Python.

We introduce the following tessellations of the computational domain $[-L, L]$, see Figure A.26:

- we consider a set of $(N+1)$ points $x_0 = -L < x_1 < \cdots < x_{N-1} < x_N = L$. Let $\mathscr{M}_{i+\frac{1}{2}} = [x_i, x_{i+1}]$, $i \in \{0, \cdots, N-1\}$, stand for the associated cells. It defines the primal mesh.

- let $x_{i+\frac{1}{2}} = \frac{(x_i + x_{i+1})}{2}$, $i \in \{0, N-1\}$ be the centers of the mesh. These points define the dual mesh made of the cells $\mathscr{M}_i = [x_{i-\frac{1}{2}}, x_{i+\frac{1}{2}}]$, $i \in \{1, \cdots, N-1\}$;

- the mesh sizes are thus given by

$$h_{i+\frac{1}{2}} = x_{i+1} - x_i, \ i \in \{0, ..., N-1\},$$
$$h_i = \frac{h_{i-\frac{1}{2}} + h_{i+\frac{1}{2}}}{2} = x_{i+\frac{1}{2}} - x_{i-\frac{1}{2}}, \ i \in \{1, ..., N-1\},$$

  (with the specific definition for the end-mesh: $h_0 = \frac{1}{2} h_{\frac{1}{2}}$ and $h_N = \frac{1}{2} h_{N-\frac{1}{2}}$).

Volume fractions and concentrations satisfy reaction-convection-diffusion equation that generically read

$$\partial_t X + \partial_x \mathscr{J} = R.$$

The discrete volume fractions and concentrations are stored on the primal mesh: given the time step δt, the $X_{i+\frac{1}{2}}$'s are updated by

$$X_{i+\frac{1}{2}}^{n+1} = X_{i+\frac{1}{2}}^{n} - \frac{\delta t}{h_{i+\frac{1}{2}}}(\mathscr{J}_{i+1} - \mathscr{J}_i) + \delta t R_{i+\frac{1}{2}},$$

for $i \in \{0..., N-1\}$. The reaction term is a function of the unknowns X; hence we simply use $R_{i+\frac{1}{2}} = R(X_{i+\frac{1}{2}}^n)$ and it remains to define the numerical fluxes $\mathscr{J}_i$, $\mathscr{J}_{i+1}$ at the interfaces of the cell $\mathscr{M}_{i+\frac{1}{2}}$. To this end, velocity fields are stored on the dual grid, and the corresponding convection fluxes are based on the upwinding principles. Therefore, the convection flux $\mathscr{J}^c = \eta X$ at the interface x_i is approached by

$$\mathscr{J}_i^c = -[\eta_i^n]_- X_{i+\frac{1}{2}}^{n+1} + [\eta_i^n]_+ X_{i-\frac{1}{2}}^{n+1}, \qquad [\eta]_\pm = \max(0, \pm\eta) \geq 0.$$

The diffusion flux $\mathscr{J}^d = -\nu \partial_x X$ at the interface x_i is approached by using a centered approximation for the derivative; namely, we get

$$\mathscr{J}_i^d = -\nu_i^n \frac{X_{i+\frac{1}{2}}^{n+1} - X_{i-\frac{1}{2}}^{n=1}}{h_i}.$$

For the sake of readability, from now on we focus on the (**T.E.O.**) model for which the coupling is simpler. The adaptation to the more complete systems is straightforward. The diffusion coefficient ν depends non linearly on the unknown X, and we set

$$\nu_i^n = \nu(X_i^n), \qquad X_i^n = \frac{X_{i+\frac{1}{2}}^n + X_{i-\frac{1}{2}}^n}{2}.$$

For stability reasons, we use a semi-implicit scheme: the field X is updated by solving a linear system, which has a reasonable numerical cost, and we can use larger time steps. Note that the preservation of the positivity of the $X_{i+\frac{1}{2}}$ might impact the choice of the time step due to the explicit discretization of the reaction term.

We turn to the discretization of the system for the velocity-pressure pair (V, Π), which reads

$$\begin{cases} -\varpi \partial_{xx}^2 V + \partial_x \Pi = F_1, \\ \\ \partial_x V - \partial_x \left(\psi \partial_x \Pi\right) = F_2. \end{cases} \tag{A.1}$$

The system is completed by the boundary conditions

$$\begin{aligned}&\partial_x\Pi(t,0)=\partial_x\Pi(t,L)=0,\\&V(t,0)=-V(t,L)=\frac{1}{2}\int_0^L R(t,x)\mathrm{d}x.\end{aligned}$$

The coefficients and source terms of the system are defined from the volume fractions:

$$\begin{aligned}&\psi=\psi(X), && R=R(X),\\&F_1=-\partial_x\mathscr{Q}(X), && F_2=R(X)+\partial_x\left(\nu(X)\partial_x X\right).\end{aligned}$$

The discrete pressure is stored on the primal mesh, while the discrete velocity, and thus the pressure gradient, are stored on the dual mesh. In turn, the convection field $\eta=V-\frac{1}{\lambda(1-X)}\partial_x\Pi$ is approached on the interface x_i by

$$\eta_i^n=V_i^n-\frac{\Pi_{i+\frac{1}{2}}^n-\Pi_{i+\frac{1}{2}}^n}{\lambda(1-X_i^n)h_i}.$$

Finally, the discrete form of (A.1) becomes

$$\begin{aligned}&-\varpi\left(\frac{V_{i+1}^n-V_i^n}{h_{i+\frac{1}{2}}}-\frac{V_i^n-V_{i-1}^n}{h_{i-\frac{1}{2}}}\right)+\Pi_{i+\frac{1}{2}}-\Pi_{i-\frac{1}{2}}=h_iF_{1,i},\\&V_{i+1}^n-V_i^n-\left(\psi_{i+1}\frac{\Pi_{i+\frac{3}{2}}-\Pi_{i+\frac{1}{2}}}{h_{i+1}}-\psi_i\frac{\Pi_{i+\frac{1}{2}}-\Pi_{i-\frac{1}{2}}}{h_i}\right)=h_{i+\frac{1}{2}}F_{2,i+\frac{1}{2}}.\end{aligned}$$

Here, we have set $\psi_i=\frac{\psi_{i+\frac{1}{2}}+\psi_{i-\frac{1}{2}}}{2}$ and the system is endowed with the boundary conditions $\psi_{-\frac{1}{2}}=0=\psi_{N+\frac{1}{2}}$, $\Pi_{-\frac{1}{2}}=\Pi_{\frac{1}{2}}$, $\Pi_{N-\frac{1}{2}}=\Pi_{N+\frac{1}{2}}$. The source terms are defined by

$$\begin{aligned}&F_{1,i}=-\frac{\mathscr{Q}(X_{i+\frac{1}{2}}^n)-\mathscr{Q}(X_{i-\frac{1}{2}}^n)}{h_i},\\&F_{2,i+\frac{1}{2}}=R(X_{i+\frac{1}{2}}^n)+\frac{1}{h_{i+\frac{1}{2}}}\left(\nu_{i+1}^n\frac{X_{i+\frac{3}{2}}^n-X_{i+\frac{1}{2}}^n}{h_{i+1}}-\nu_i^n\frac{X_{i+\frac{1}{2}}^n-X_{i-\frac{1}{2}}^n}{h_i}\right).\end{aligned}$$

The boundary conditions for the velocity is defined by using a suitable quadrature formula (rectangle or trapezoidal rule) for approaching the integral of the reaction term.

As said above, the numerical strategy is adapted from [20, 46]. However, the scheme is based on a specific formulation of the continuous system, and it is not clear that it preserves the equivalent expressions of the incompressibility constraints. For further details on this issue and on more elaborate versions of the scheme, we refer the reader to [9, 51].

Appendix B. Dimension of the quantities of interest

Complementing Table 1 and Table 2, we provide below the dimensions of the quantities involved in the equations, even if the simulations are performed in dimensionless form.

References

[1] L. Almeida, C. Audebert, E. Leschiera, and T. Lorenzi. A hybrid discretecontinuum modelling approach to explore the impact of T-cell infiltration on anti-tumour immune response. *Bull. Math. Biol.*, 84:141, 2022.

[2] P. Altea-Manzano, A. M. Cuadros, L. A. Broadfield, and S.-M. Fendt. Nutrient metabolism and cancer in the in vivo context: a metabolic game of give and take. *EMBO Rep.*, 21(10):e50635, 2020.

[3] D. Ambrosi and L. Preziosi. On the closure of mass balance models for tumor growth. *Math. Mod. Meth. Appl. Sci.*, 12(5):737–754, 2002.

[4] N. M. Anderson and M. Celeste Simon. The tumor microenvironment. *Current Biology*, 30:R905R931, 2020.

[5] K. Atsou, F. Anjuère, V. Braud, and T. Goudon. A size and space structured model of tumor growth describes a key role for protumor immune cells in breaking equilibrium states in tumorigenesis. *PlosOne*, page 0259291, 2021.

[6] K. Atsou, F. Anjuère, V. M. Braud, and T. Goudon. A size and space structured model describing interactions of tumor cells with immune cells reveals cancer persistent equilibrium states in tumorigenesis. *J. Theor. Biol.*, 490:110163, 2020.

Variable	Unit
t	time in day
x	space in mm
V	$mm \cdot day^{-1}$
ϕ	dl
I	dl
O	dl
Φ	dl
ρ	$g \cdot mm^{-d}$ x
p_*, Π	$mm^2 \cdot day^{-2}$
D_Φ	$g \cdot mm^{2-d}$
$\chi_{a,p},\ D_{a,p}$	$mm^2 \cdot day^{-2}$
$\chi_O,\ D_O$	$mm^2 \cdot day^{-1}$
γ	day^{-1}
A_a	dl
$S_{a,p}$	dl
S_O	day^{-1}
g_0	day^{-1}
$k_{I_p},\ k_{I_a}$	day^{-1}
r	$mm^d \cdot g^{-1} \cdot day^{-1}$
f_*	day^{-1}
$\phi_{n_{I,s}}$	dl
τ	day
λ	day^{-1}
ϖ_m	$g \cdot mm^{-1} \cdot day^{-1}$

Table B.4: Physical dimensions of the variables and parameters ($d \in \{1, 2, 3\}$ stands for the considered space dimension and dl means dimensionless)

[7] K. Atsou, F. Anjuère, V. M. Braud, and T. Goudon. Analysis of the equilibrium phase in immune-controlled tumors provides hints for designing better strategies for cancer treatment. *Front. Oncol.*, page 2022.878827, 2022.

[8] M. Basan, T. Risler, J.-F. Joanny, X. Sastre-Garau, and J. Prost. Homeostatic competition drives tumor growth and metastasis nucleation. *HSFP J.*, 3(4):265–272, 2009.

[9] O. Bernard, M. Bestard, T.Goudon, L. Meyer, S. Minjeaud, F. Noisette, and B. Polizzi. Numerical schemes for mixture theory models with filling constraint: application to biofilm ecosystems. Technical report, Univ. Côte d'Azur, CNRS, Inria, LJAD, 2023.

[10] M. Binnewies, E.W. Roberts, K. Kersten, V. Chan, D. F. Fearon, M. Merad, L. M. Coussens, D. I. Gabrilovich, S. Ostrand-Rosenberg, C. C. Hedrick, R. H. Vonderheide, M. J. Pittet, R. K. Jain, W.Zou, T. K. Howcroft, E. C. Woodhouse, R. A. Weinberg, and M. F. Krummel. Understanding the tumor immune microenvironment (TIME) for effective therapy. *Nature Medicine*, 24:541–550, 2018.

[11] M. A. Boemo and H. M. Byrne. Mathematical modelling of a hypoxia-regulated oncolytic virus delivered by tumour-associated macrophages. *J. Theor. Biol.*, 461:102116, 2019.

[12] P. Bourdely, L. Petti, J. Cazareth, A. Meghraoui-Kheddar, E. Elaldi, S. Khou, A. Rubod, G. Poissonnet, A. Sudaka, V. M. Braud, and F. Anjuère. Autofluorescence discriminates functionally distinct macrophages subsets in mouse skin and human cutaneous squamous cell carcinoma using spectral flow cytometry. Technical report, Univ. Côte d'Azur, CNRS, Inserm, 2021. Submitted.

[13] D. Bresch, T. Colin, E. Grenier, B. Ribba, and O. Saut. Computational modeling of solid tumor growth: the avascular stage. *SIAM J. Sci. Comput.*, 32(4):2321–2344, 2010.

[14] C. J. W. Breward, H. M. Byrne, and C. E. Lewis. A multiphase model describing vascular tumour growth. *Bull. Math. Biol.*, 65:609–640, 2003.

[15] H. Byrne and D. Drasdo. Individual-based and continuum models of growing cell populations: a comparison. *J. Math. Biol.*, 58:657–687, 2009.

[16] H. M. Byrne. Multiphase modelling in cancer. Lectures CRM Barcelona, 2018.

[17] H. M. Byrne and L. Preziosi. Modelling solid tumour growth using the theory of mixtures. *Math. Med. Biol.*, 20(4):341–366, 2003.

[18] C. Carmona-Fontaine, M. Deforet, L. Akkari, C. B. Thompson, J. A. Joyce, and J. B. Xavier. Metabolic origins of spatial organization in the tumor microenvironment. *PNAS Biol. Sci.*, 114(11):2934–2939, 2017.

[19] C. Y. Chen, H. M. Byrne, and J. R. King. The influence of growth-induced stress from the surrounding medium on the development of multicell spheroids. *J. Math. Biol.*, 43:191–220, 2001.

[20] F. Clarelli, C. Di Russo, R. Natalini, and M. Ribot. A fluid dynamics model of the growth of phototrophic biofilms. *J. Math. Biol.*, 66:1387–1408, 2013.

[21] T. Colin, O. Gallinato, C. Poignard, and O. Saut. Tumor growth model for ductal carcinoma: from in situ phase to stroma invasion. *J. Theor. Biol.*, 429:253–266, 2017.

[22] V. Cristini, X. Li, J. S. Lowengrub, and S. M. Wise. Nonlinear simulations of solid tumor growth using a mixture model: invasion and branching. *J. Math. Biol.*, 58:article # 723, 2009.

[23] N. David and B. Perthame. Free boundary limit of a tumor growth model with nutrient. *J. Math. Pures Appl.*, 155:62–82, 2021.

[24] L. G. de Pillis, D. G. Mallet, and A. E. Radunskaya. Spatial tumor-immune modeling. *Comput. Math. Methods Medicine*, 7(2-3):159–176, 2006.

[25] L. G. de Pillis, A. E. Radunskaya, and C. L. Wiseman. A validated mathematical model of cell-mediated immune response to tumor growth. *Cancer Res.*, 65(17):7950–7958, 2005.

[26] L.G. de Pillis and A. Radunskaya. The dynamics of an optimally controlled tumor model: A case study. *Math. Comput. Modelling*, 37:1221–1244, 2003.

[27] C. Draghi, L.Viger, F. Denis, and C. Letellier. How the growth rate of host cells affects cancer risk in a deterministic way. *Chaos*, 27:093101, 2017.

[28] G. P. Dunn, A. T. Bruce, H. Ikeda, L. J. Old, and R. D. Schreiber. Cancer immunoediting: from immunosurveillance to tumor escape. *Nat. Immunol.*, 3:991998, 2002.

[29] G. P. Dunn, L. J. Old, and R. D. Schreiber. The immunobiology review of cancer immunosurveillance and immunoediting. *Immunity*, 21:137–148, 2004.

[30] R. Eftimie, J. L. Bramson, and D. J. D. Earn. Interactions between the immune system and cancer: A brief review of non-spatial mathematical models. *Bull. Math. Biol.*, 73(1):2–32, Jan 2011.

[31] R. Eftimie, J. J. Gillard, and D. A. Cantrell. Mathematical models for immunology: current state of the art and future research directions. *Bull. Math. Biol.*, 78:2091–2134, 2017.

[32] R. Elaldi, P. Hemon, L. Petti, E. Cosson, B. Desrues, A. Sudaka, G. Poissonnet, E. Van Obberghen-Schilling, J.-O. Pers, V. M. Braud, F. Anjuère, and A. Meghraoui-Kheddar. High dimensional imaging mass cytometry panel to visualize the tumor immune microenvironment contexture. *Front. Immunol.*, 12:666233, 2021.

[33] Harlow F. H. and J. E. Welch. Numerical calculation of time-dependent viscous incompressible flow of fluid with free surface. *Phys. Fluids*, 8(12):2182–2189, 1965.

[34] D. Hanahan and R. A. Weinberg. Hallmarks of cancer: The next generation. *Cell*, 144:646–674, 2011.

[35] T. Jackson and H. M. Byrne. A mechanical model of tumor encapsulation and transcapsular spread. *Math. Biosci.*, 180:307–328, 2002.

[36] N. Kedia-Mehta and D. K. Finlay. Competition for nutrients and its role in controlling immune responses. *Nature Comm.*, page 10:2123, 2019.

[37] S. Khou, A. Popa, C. Luci, F. Bihl, A. Meghraoui-Kheddar, P. Bourdely, E. Salavagione, E. Cosson, A. Rubod, J. Cazareth, P. Barbry, B. Mari, Rezzonico R., F. Anjuère, and V.M. Braud. Tumor-associated neutrophils dampen adaptive immunity and promote cutaneous squamous cell carcinoma development. *Cancers*, 12(7):1860, 2020.

[38] D. E. Kirschner and J. C. Panetta. Modeling immunotherapy of the tumor-immune interaction. *J. Math. Biol.*, 37:235–252, 1998.

[39] V. Kuznetsov and G. Knott. Modelling tumor regrowth and immunotherapy. *Math. Comput. Modelling*, 33(12/13):1275–1287, 2001.

[40] S. Labarthe, B. Polizzi, T. Phan, T. Goudon, M. Ribot, and B. Laroche. A mathematical model to investigate the key drivers of the biogeography of the colon microbiota. *J. Theor. Biol.*, 462:552–581, 2019.

[41] K.-L. Liao, X.-F. Bai, and A. Friedman. Mathematical modeling of interleukin-35 promoting tumor growth and angiogenesis. *PlosOne*, 9(10):e110126, 2014.

[42] C. Luci, F. Bihl, P. Bourdely, S. Khou, A. Popa, A. Meghraoui-Kheddar, O. Vermeulen, R. Elaldi, G. Poissonnet, A. Sudaka, R. Rezzonico, S. Bekri, J. Cazareth, G. Ponzio, P. Barbry, B. Mari, V.M. Braud, and F. Anjuère. Cutaneous squamous cell carcinoma development is associated with a temporal infiltration of ILC1 and NK cells with immune dysfunctions. *J. Invest. Dermatol.*, 141(10):2369–2379, 2021.

[43] P. Macklin, S. McDougall, A. R. A. Anderson, M. A. J. Chaplain, V. Cristini, and J.Lowengrub. Multiscale modelling and nonlinear simulation of vascular tumour growth. *J. Math. Biol.*, 58:765–798, 2009.

[44] H. T. Nia, H. Liu, G. Seano, M. Datta, D. Jones, N. Rahbari, J. Incio, V. P. Chauhan, K. Jungand J. D. Martin, and T. P. Paderaand D. Fukumura V. Askoxylakis, Y. Boucher, and L. L. Munn F. J. Hornicekand A. J. Grodzinsky, and J. W. Baish, and R. K. Jain. Solid stress and elastic energy as measures of tumour mechanopathology. *Nature Biomed. Eng.*, 1:0004, 2016.

[45] B. Perthame, F. Quirós, and J.-L. Vázquez. The Hele-Shaw asymptotics for mechanical models of tumor growth. *Arch. Rat. Mech. Anal.*, 212:93–127, 2014.

[46] B. Polizzi, O. Bernard, and M. Ribot. A time-space model for the growth of microalgae biofilms for biofuel production. *J. Theor. Biol.*, 432:55–79, 2017.

[47] L. Preziosi and A. Farina. On Darcy's law for growing porous media. *Int. J. Non-Linear Mech.*, 37(3):485–491, 2002.

[48] L. Preziosi and A. Tosin. Multiphase modelling of tumour growth and extracellular matrix interaction: mathematical tools and applications. *J. Math. Biol.*, 58(4-5):625–656, 2009.

[49] K. R. Rajagopal and L. Tao. *Mechanics of Mixtures*. World Scientific, 1995.

[50] T. Roose, S. J. Chapman, and P. K. Maini. Mathematical models of avascular tumor growth. *SIAM Rev.*, 49(2):179–208, 2007.

[51] C. Tayou Fotso. *Modélisation des interactions entre croissance tumorale et réponse immunitaire*. PhD thesis, Univ. Côte d'Azur. Work in preparation.

[52] J. O. Waldeland, W. J. Polacheck, and S. Evje. Collective tumor cell migration in the presence of fibroblasts. *J. Biomech.*, 100:109568, 2020.

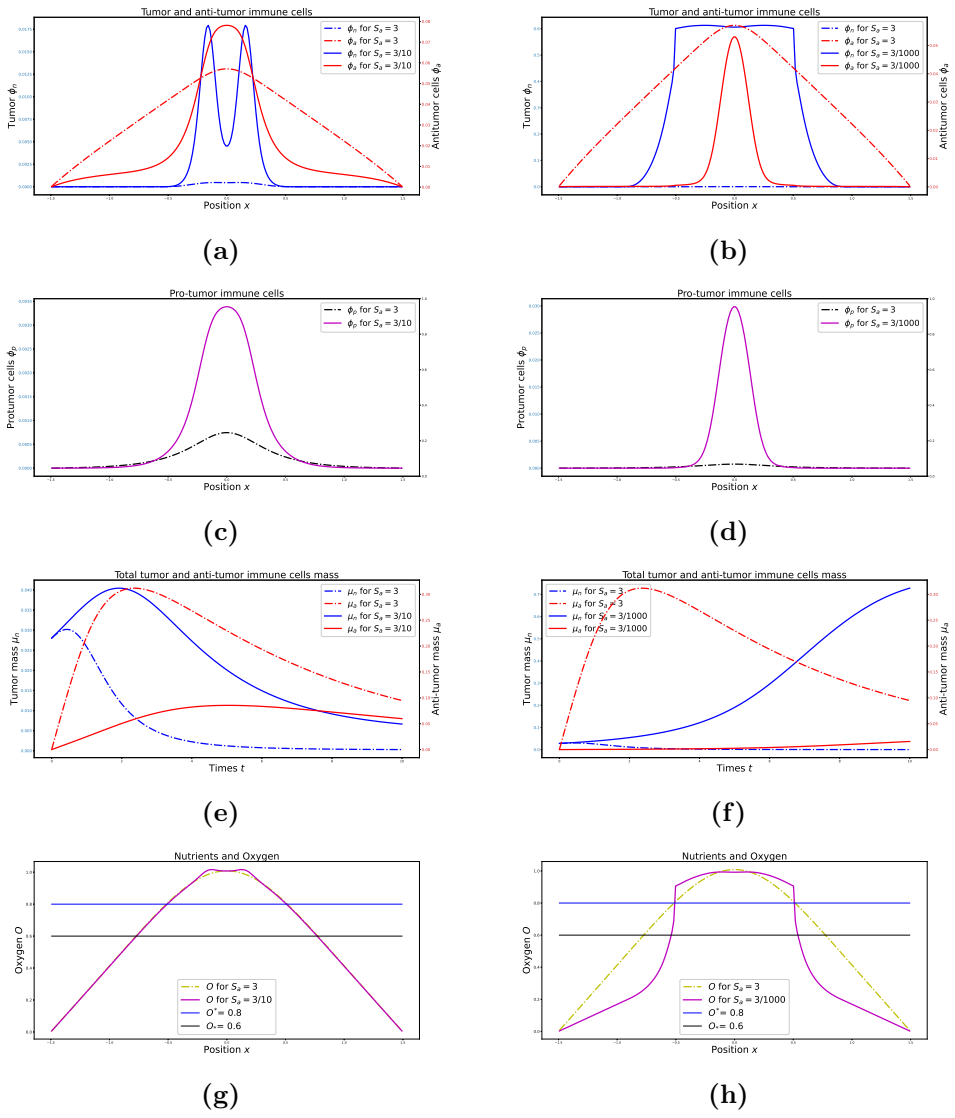

Figure 14: Simulation of the model (**Full**): profile of the tumor, anti- and protumor cells volume fraction ϕ_n, ϕ_a and ϕ_p, the oxygen concentration O and time evolution of the total mass of the tumor μ_n and antitumor cells μ_a for different values of S_a. (a-c-e-g): $S_a = 3$ and $S_a = 3/10$, (b-d-f-h): $S_a = 3$ and $S_a = 3/1000$, with $S_p = 3$, $\chi_O = 1$, $f_* = 1$, and $\tau = 1/1000$ (relaxation time for cytokines). The parameters of the simulations are: $O^* = .8$ (proliferation threshold), $O_* = .6$ (necrotic threshold), and S_O given by (20b), $\nu = 50$, $A_a = 5$, $r_n = .9$, $r_m = r_a = r_p = r_n/10$

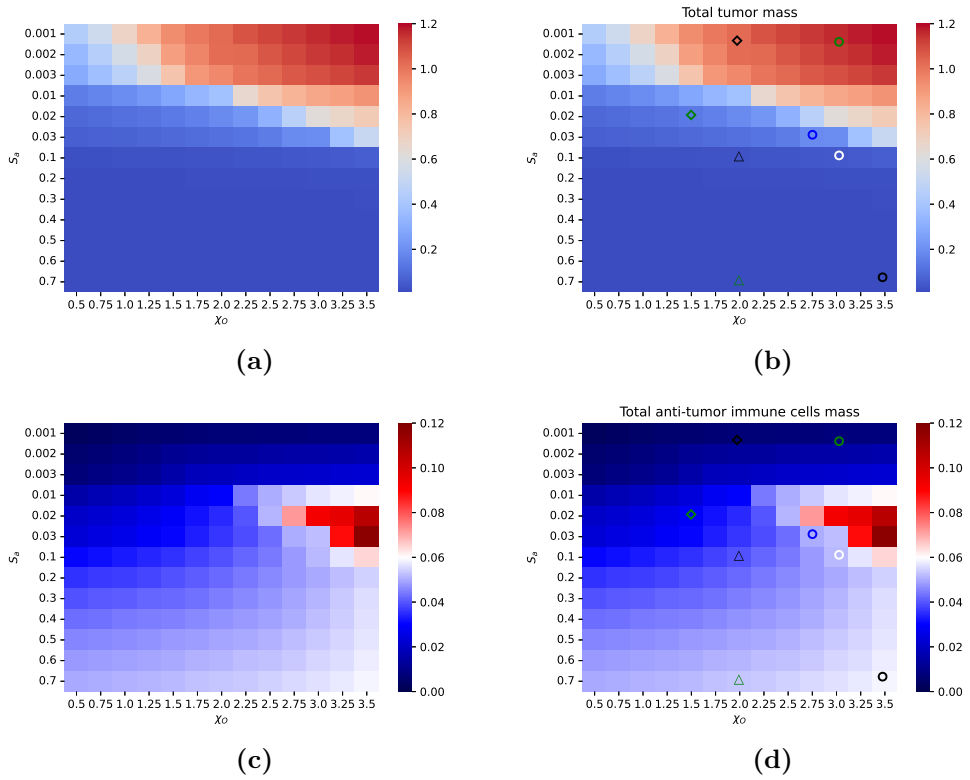

Figure 15: Heat map of the mean total tumor mass (a, b) and mean total mass of antitumor immune cells (c, d) over time, with final time $T = 100$ (a,c) or $T = 200$ (b,d), for the coupled model (**T.A.E.O.**), depending on the chemotactic coefficient and the amplitude of the source of antitumor immune cells (χ_O, S_a). The time evolution of the marked areas in (b-d) will be displayed below.

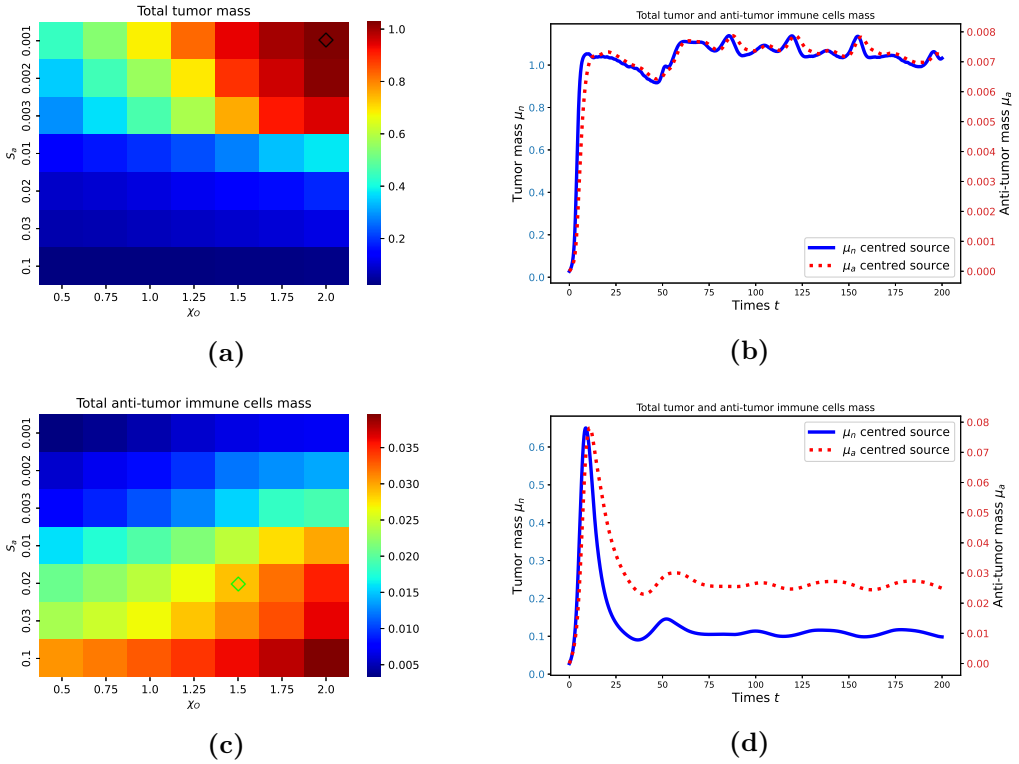

Figure 16: Heat map for the coupled model (**T.A.E.O.**). In (a) and (c): zoom on the domain $\chi_O \in [0.5; 2]$, $S_a \in [10^{-3}; 0.1]$ from Figures 15.b) and 15.d). In (b): time evolution of the total mass of tumor and antitumor immune cells μ_n and μ_a for $(\chi_O; S_a) = (2; 10^{-3})$, point spotted in (a), an example of escape, and in (d): $(\chi_O; S_a) = (1.5; 0.02)$, point spotted in (c), an example of equilibrium with residual tumor

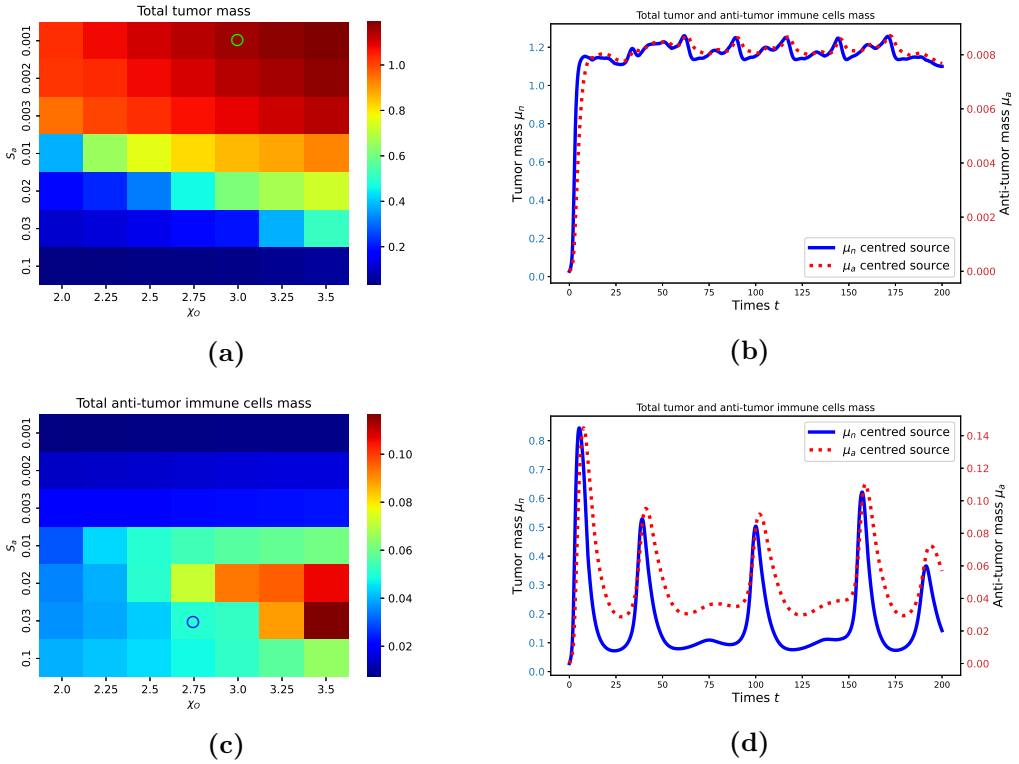

Figure 17: Heat map for the coupled model (**T.A.E.O.**). In (a) and (c): zoom on the domain $\chi_O \in [2; 3.5]$, $S_a \in [10^{-3}; 0.1]$ from Figures 15.b) and 15.d). In (b): time evolution of the total mass of tumor and antitumor immune cells μ_n and μ_a for $(\chi_O; S_a) = (3; 10^{-3})$, point spotted in (a), an example of escape, and in (d): $(\chi_O; S_a) = (2.75; 0.03)$ point spotted in (c), an example with slightly damped oscillations

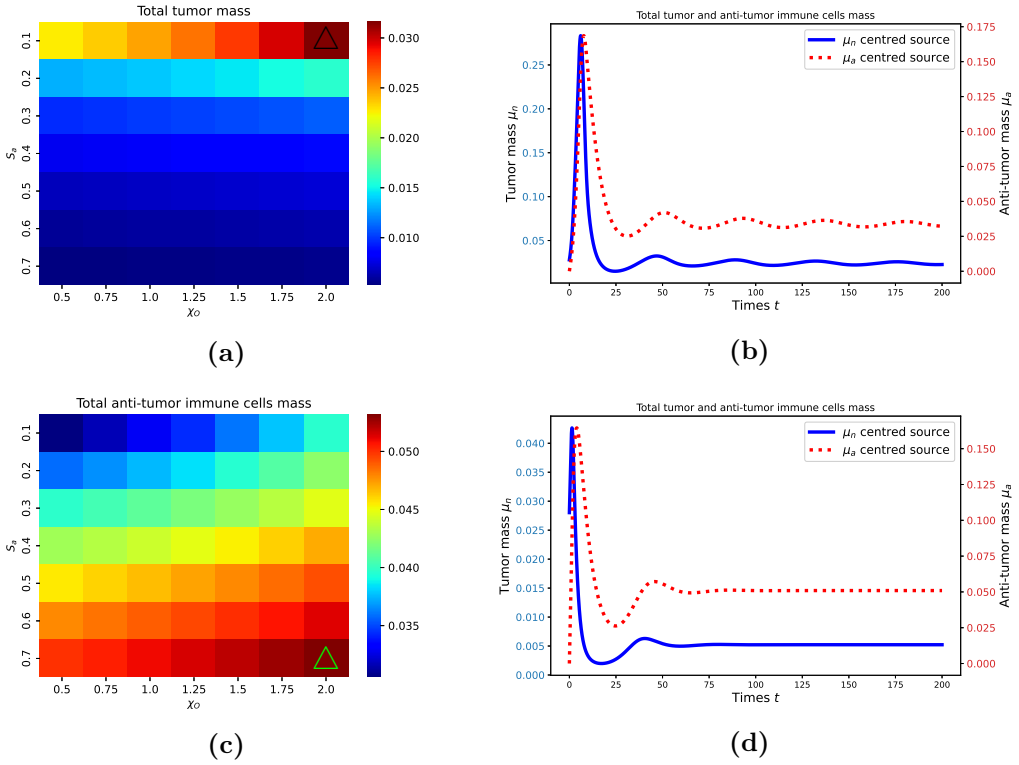

Figure 18: Heat map for the coupled model (**T.A.E.O.**). In (a) and (c): zoom on the domain $\chi_O \in [0.5; 2]$, $S_a \in [0.1; 0.7]$ from Figures 15.b) and 15.d). In (b): time evolution of the total mass of tumor and antitumor immune cells μ_n and μ_a for $(\chi_O; S_a) = (2; 0.1)$ point spotted in (a), and in (d): $(\chi_O; S_a) = (2; 0.7)$, point spotted in (c): two examples of equilibrium with a residual tumor

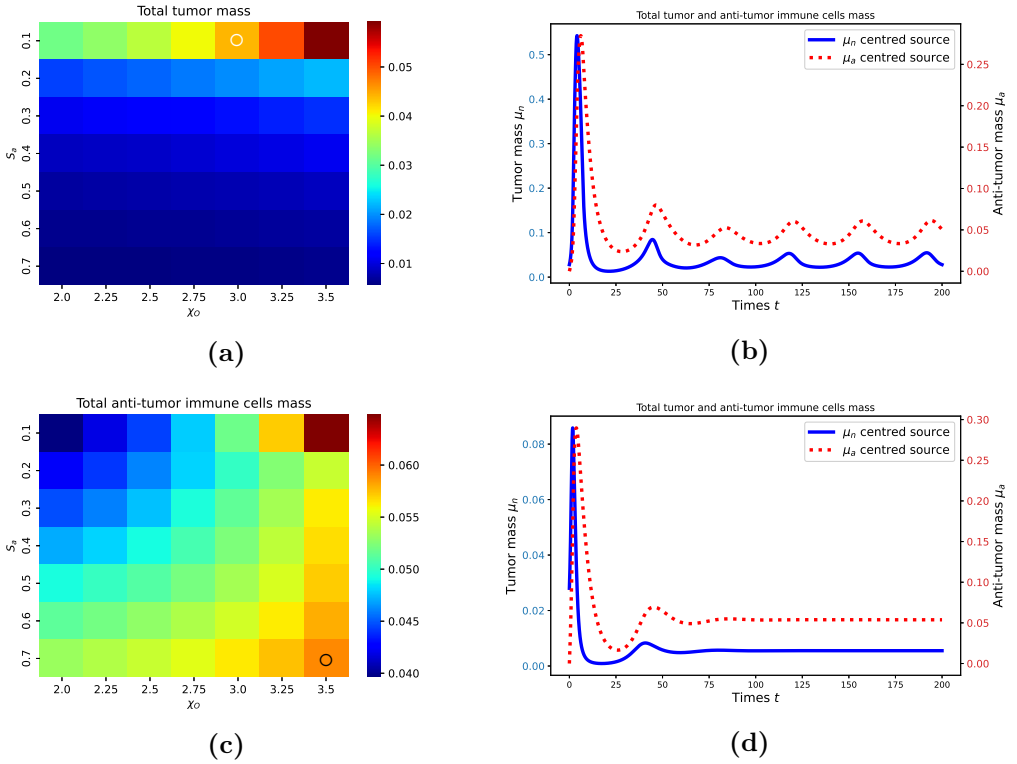

Figure 19: Heat map for the coupled model (**T.A.E.O.**). In (a) and (c): zoom on the domain $\chi_O \in [2; 3.5]$, $S_a \in [0.1; 0.7]$ from Figures 15.b) and 15.d). In (b): time evolution of the total mass of tumor and antitumor immune cells μ_n and μ_a for $(\chi_O; S_a) = (3; 0.1)$, point spotted in (a), and in (d): $(\chi_O; S_a) = (3.5; 0.7)$, point spotted in (c): two examples of equilibrium with a residual tumor

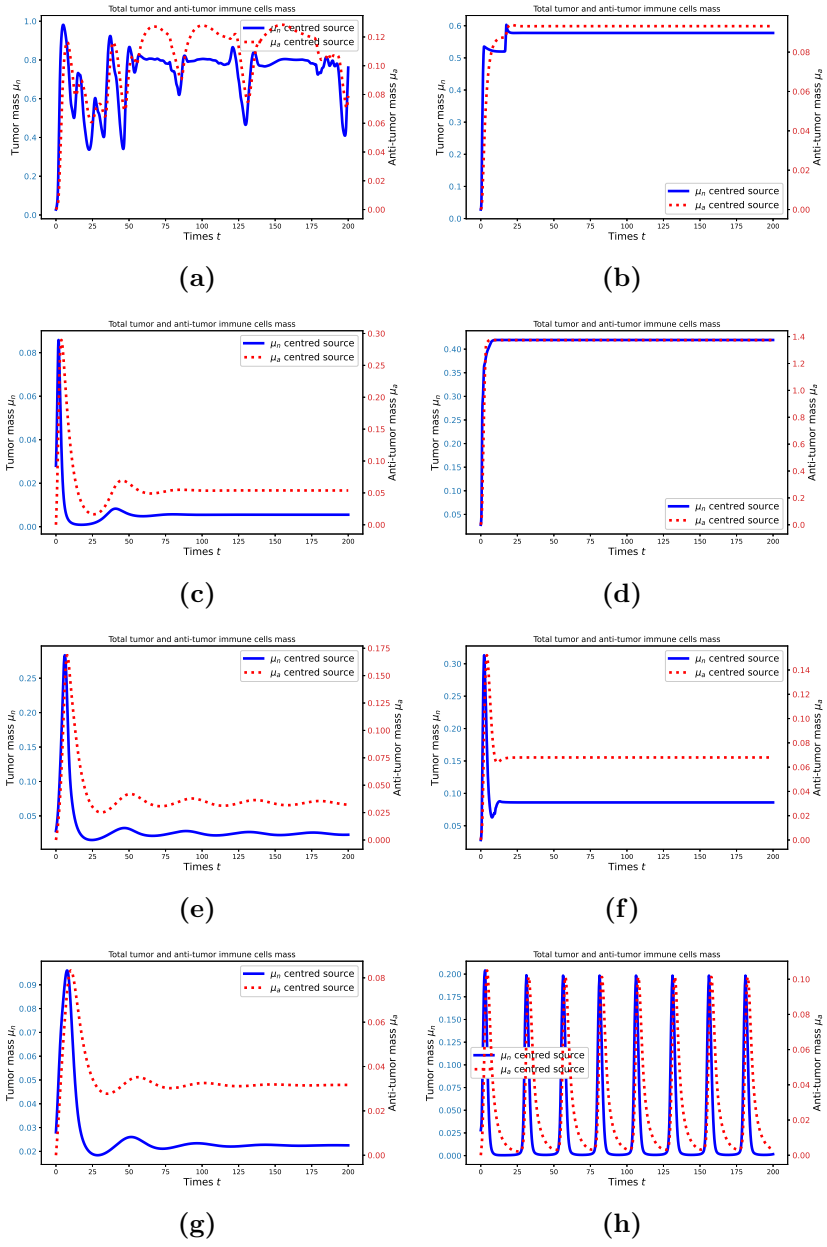

Figure 20: Simulation of the coupled model (**T.A.E.O.**), time evolution of total tumor and antitumor immune cells mass for several pairs of chemotactic coefficient and amplitude of the source of immune cells: $(\chi_O; S_a) = (3.5; 2 \times 10^{-2})$ for (a-b), $(\chi_O; S_a) = (3.5; 0.7)$ for (c-d), $(\chi_O; S_a) = (2; 0.1)$ for (e-f), $(\chi_O; S_a) = (1.25; 0.1)$ for (g-h): with $f_* = 0$ for (a, c, e, g), $f_* = 1$ for (b, d, f, h). The degradation of the environment $f_* \neq 0$ favors the tumor development and reduces the antitumor effects of the immune response

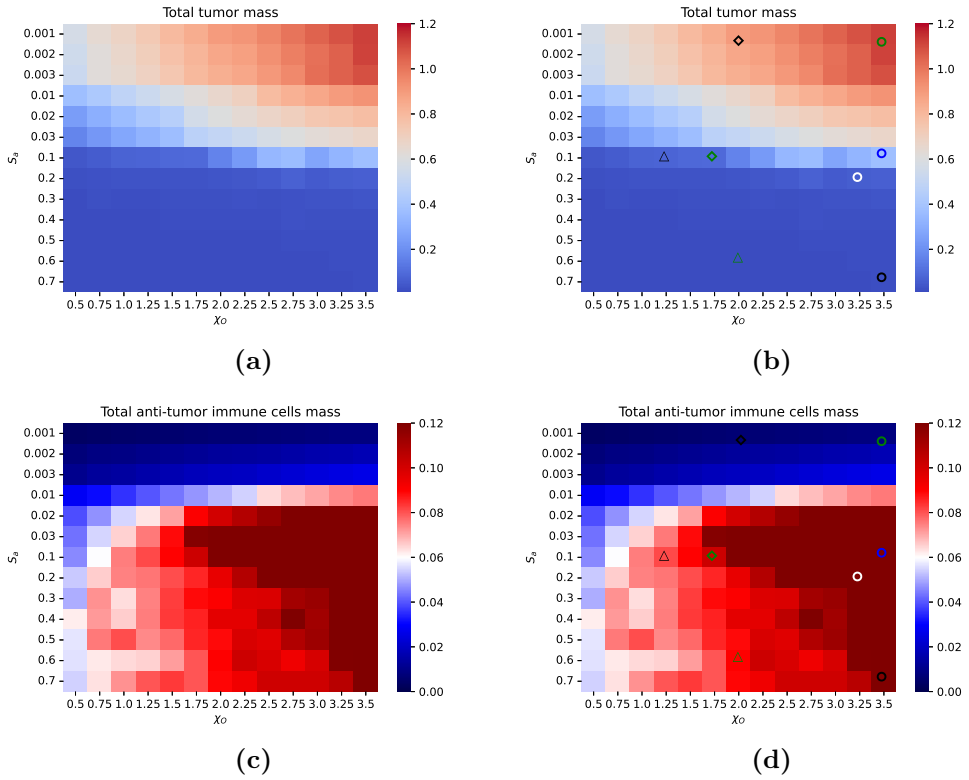

Figure 21: Heat map of the mean total tumor mass (a, b) and mean total mass of antitumor immune cells (c, d) over time, with final time $T = 100$ (a,c) or $T = 200$ (b,d), for the coupled model (**Full**), depending on the chemotactic coefficient and the amplitude of the source of antitumor immune cells (χ_O, S_a). The time evolution of the marked areas in (b-d) will be displayed below

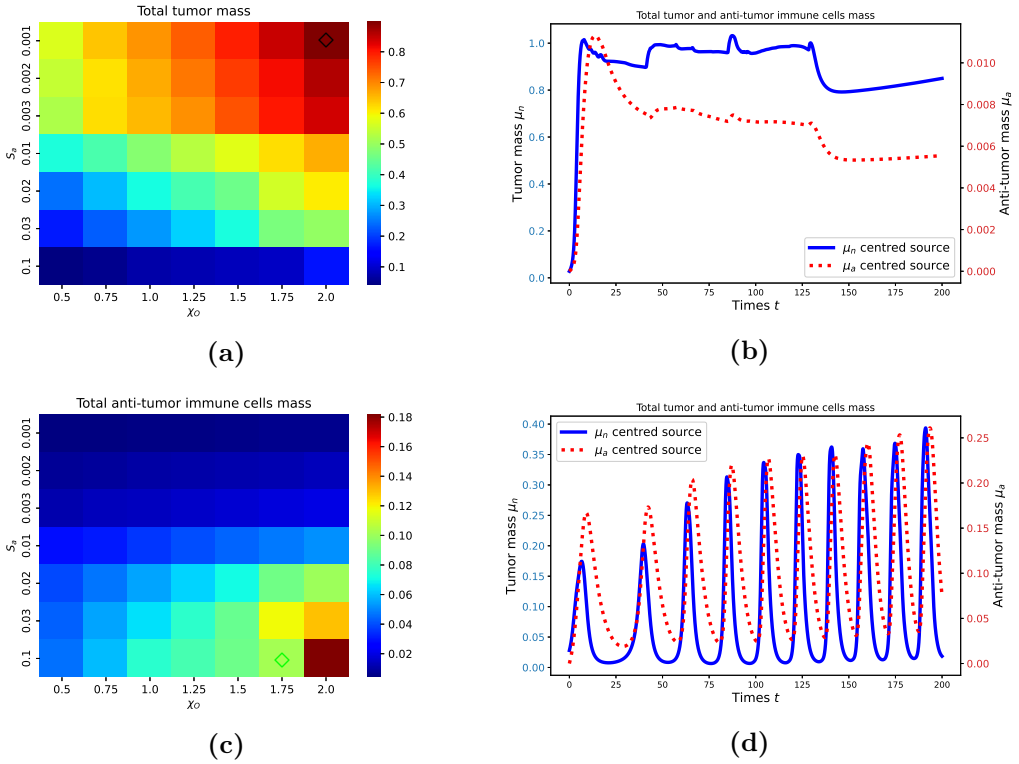

Figure 22: Heat map for the coupled model (**Full**). In (a) and (c): zoom on the domain $\chi_O \in [0.5; 2]$, $S_a \in [10^{-3}; 0.1]$ from Figures 21.b) and 21.d). In (b): time evolution of the total mass of tumor and antitumor immune cells μ_n and μ_a for $(\chi_O; S_a) = (2; 10^{-3})$, point spotted in (a), an example of escape, and in (d): $(\chi_O; S_a) = (1.75; 0.1)$, point spotted in (c), an example of amplified oscillations

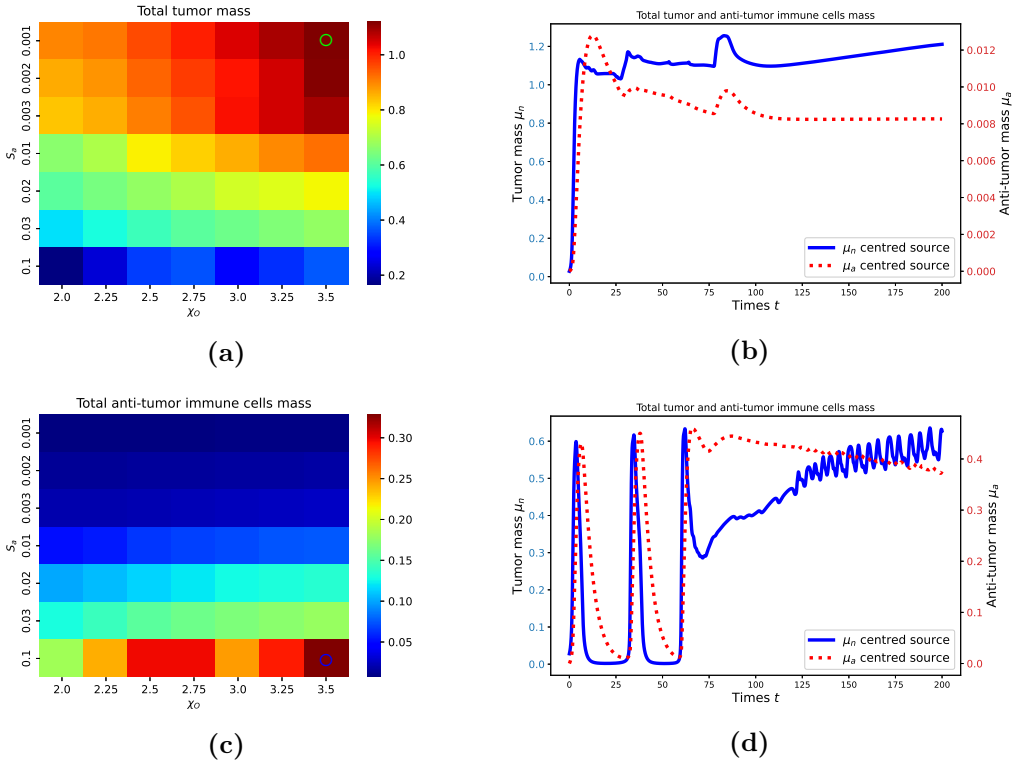

Figure 23: Heat map for the coupled model (**Full**). In (a) and (c): zoom on the domain $\chi_O \in [2; 3.5]$, $S_a \in [10^{-3}; 0.1]$ from Figures 21.b) and 21.d). In (b): time evolution of the total mass of tumor and antitumor immune cells μ_n and μ_a for $(\chi_O; S_a) = (3.5; 10^{-3})$, point spotted in (a), and in (d): $(\chi_O; S_a) = (3.5; 0.1)$, point spotted in (c), two examples of escape

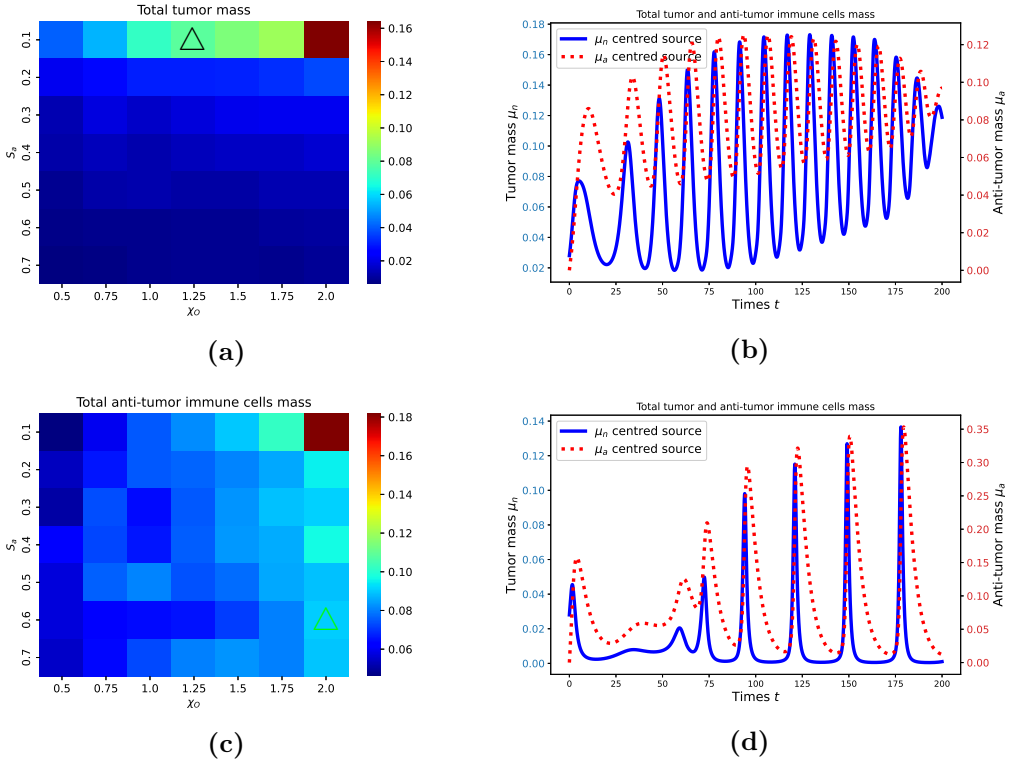

Figure 24: Heat map for the coupled model (**Full**). In (a) and (c): zoom on the domain $\chi_O \in [0.5; 2]$, $S_a \in [0.1; 0.7]$ from Figures 21.b) and 21.d). In (b): time evolution of the total mass of tumor and antitumor immune cells μ_n and μ_a for $(\chi_O; S_a) = (1.25; 0.1)$, point spotted in (a), and in (d): $(\chi_O; S_a) = (2; 0.6)$, point spotted in (c): while the mean tumor mass remains moderate, we observe oscillations of significantly high values for the tumor mass

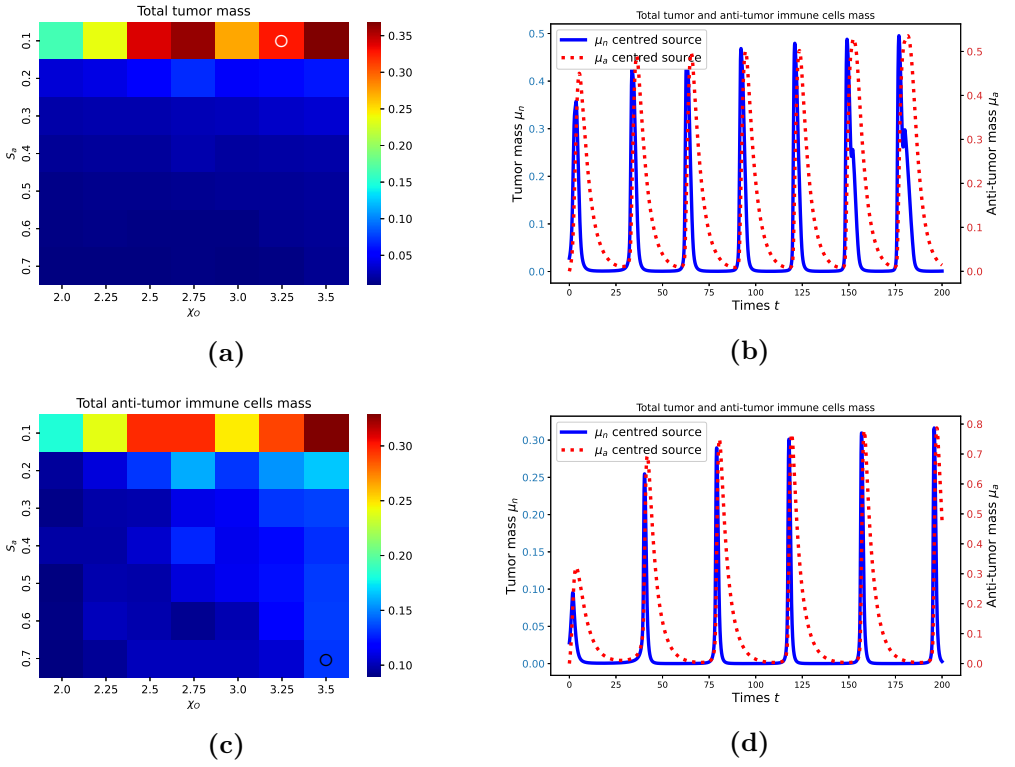

Figure 25: Heat map for the coupled model (**Full**). In (a) and (c): zoom on the domain $\chi_O \in [2; 3.5]$, $S_a \in [0.1; 0.7]$ from Figures 21.b) and 21.d). In (b): time evolution of the total mass of tumor and antitumor immune cells μ_n and μ_a for $(\chi_O; S_a) = (3.25; 0.2)$, point spotted in (a), and in (d): $(\chi_O; S_a) = (3.5; 0.7)$, point spotted in (c): while the mean tumor mass remains moderate, we observe oscillations of significantly high values for the tumor mass

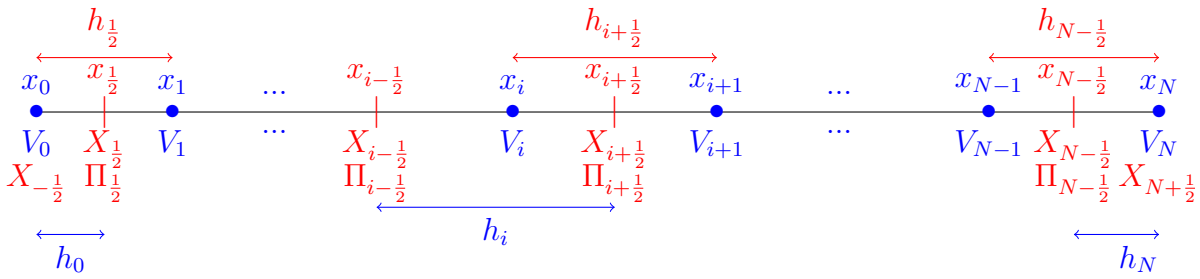

Figure A.26: Staggered grid in dimension one. In the case of a regular mesh we have: $h_{i+\frac{1}{2}} = h$ for $i \in \{0, \cdots, N-1\}$, $h_i = h$ for $i \in \{1, \cdots, N-1\}$ and $h_0 = h_N = \frac{h}{2}$.